Stabilization / destabilization of the APP transmembrane domain by mutations in the di-glycine hinge alter helical structure and dynamics, and impair cleavage by γ-secretase

Alexander Götz[1], Nadine Mylonas[2,5,*], Philipp Högel[3,*], Mara Silber[4,*], Hannes Heinel[6], Simon Menig[1], Alexander Vogel[6], Hannes Feyrer[4], Daniel Huster[6], Burkhard Luy[4], Dieter Langosch[3], Christina Scharnagl[1,#], Claudia Muhle-Goll[4,#], Frits Kamp[2], and Harald Steiner[2,5,#]

[1]Physics of Synthetic Biological Systems (E14), Technical University of Munich, Freising, Germany

[2]Biomedical Center - BMC, Metabolic Biochemistry, Ludwig-Maximilians-University, Munich, Germany

[3]Center for Integrated Protein Science Munich (CIPSM) at the Lehrstuhl Chemie der Biopolymere, Technical University Munich, Weihenstephaner Berg 3, 85354 Freising, Germany

[4]Institute of Organic Chemistry and Institute for Biological Interfaces 4, Karlsruhe Institute of Technology, Karlsruhe, Germany

[5]German Center for Neurodegenerative Diseases (DZNE), Munich, Germany

[6]Institute for Medical Physics and Biophysics, Leipzig University, Leipzig, Germany

[*] Equal contributions

[#] Corresponding authors: christina.scharnagl@tum.de; claudia.muhle-goll@kit.edu; harald.steiner@med.uni-muenchen.de

Abstract

γ-Secretase is a pivotal intramembrane protease that is involved in the generation of toxic Alzheimer´s disease-associated peptides from the β-amyloid precursor protein C-terminal fragment C99. Determinants of γ-secretase substrates are not defined yet and in the absence of recognition motifs, helix-stability and dynamics have been discussed as critical factors for recognition and cleavage of γ-secretase. Since conformational flexibility of a di-glycine hinge region in the C99 transmembrane domain (TMD), which separates the TMD into N- and C-terminal parts, might play a role in the processing of C99 by γ-secretase, we mutated one of the glycines, G38, to a helix-stabilizing leucine and to a helix-distorting proline residue. While γ-secretase cleavage of the G38L mutant was reduced, that of G38P was strongly impaired. Furthermore, cleavage precision of γ-secretase was dramatically altered by the mutations. CD and NMR spectroscopy, hydrogen/deuterium exchange measurements as well as *in silico* modeling by MD simulations to assess structural and dynamical parameters showed that the mutations affected the TMD helix properties, in particularly for the G38P mutant. However, helix destabilization was not observed at the ε-cleavage sites of C99, suggesting that local unfolding of the TMD to allow access to the scissile bonds requires the presence of the protease. Our data suggest that conformational relaxations of substrate and enzyme during substrate recruitment required for catalysis are established only when substrate and protease come into contact.

Introduction

Proteolysis in the hydrophobic core of membranes is a fundamental cellular process mediating critical signaling events as well as membrane protein turnover. Intramembrane proteases are found in all kingdoms of life and exist in several catalytic types (1). They are generally polytopic membrane proteins carrying their active sites residues in transmembrane helices (2). Apart from the fact that intramembrane cleavage occurs typically within the transmembrane domain (TMD), little is still known about the substrate determinants of intramembrane proteases. Intramembrane proteases do, with few exceptions of some rhomboid proteases, not recognize consensus sequences in substrates, like common soluble proteases such as caspases or trypsin. Rather than sequence motifs, intrinsic instability and global flexibility of substrate TMD helices that could be induced by e.g. helix-destabilizing glycine residues in case of signal peptide peptidase (SPP) (3) or the related SPP-like (SPPL) protease SPPL2b (4), or a short helix-distorting asparagine-proline motif in case of site-2 protease (5,6) are now increasingly discussed as a critical factor for substrate recognition and/or cleavage.

γ-Secretase is a pivotal intramembrane protease complex (7,8) that cleaves more than hundred type I membrane protein substrates including signaling proteins essential for life such as Notch1 as well as the β-amyloid precursor protein (APP), which is central to the pathogenesis of Alzheimer´s disease (AD) (9,10). It is widely believed that an aberrant generation and accumulation of amyloid β-peptide (Aβ) in the brain triggers the disease (11,12). Aβ is a heterogeneous mixture of secreted, small peptides of 37-43 amino acids. Besides the major form $A\beta_{40}$, the highly aggregation-prone longer forms $A\beta_{42}$ and $A\beta_{43}$ are pathogenic Aβ variants. Aβ species are generated by γ-secretase from an APP C-terminal fragment (C99) that is generated by an initial APP cleavage of β-secretase (13). C99 is first endoproteolytically cleaved in its TMD by γ-secretase at the ε-sites close to the cytoplasmic TMD border and then processed stepwise by tripeptide-releasing carboxy-terminal trimming

in two product lines ($A\beta_{40}$-line and $A\beta_{42}$-line) thereby releasing the various Aβ species (14,15). Mutations in the presenilins, the catalytic subunit of γ-secretase, are the major cause of familial forms of AD (FAD) and are associated with increased $A\beta_{42}$ to total Aβ ratios (16). Rare mutations in the cleavage region of the C99 TMD also shift Aβ profiles and represent another cause of FAD (16,17).

The molecular properties of substrates that are recognized by γ-secretase are still largely enigmatic (18). Established general substrate requirements are not only the presence of a short ectodomain, which is typically generated by sheddases such as α- or β-secretase, but, equally important, also permissive transmembrane and intracellular substrate domains (18). At the molecular level, nicastrin, the largest subunit of γ-secretase, has been suggested to provide a steric hindrance for full length proteins with large ectodomains (19) which are increasingly less well, if at all, cleaved as they increase in length over 50 amino acids (20). Recent studies suggest that the recruitment of C99 to the active site occurs in a stepwise process involving prior binding to exosites in the nicastrin, PEN-2 and presenilin-1 (PS1) N-terminal fragment subunits of γ-secretase (21). Interactions with exosites may thus provide important checkpoints of the enzyme to distinguish substrates from nonsubstrates. At the active site, productive interactions of C99 with the S2′ subsite pocket of the enzyme are critical for substrate cleavage and Aβ product line selection (15).

Kinetic studies have shown that γ-secretase cleavage of C99 is a very slow process in the minute range, i.e. much slower than soluble proteases (22). Similarly low k_{cat} values as for C99 were determined for Notch1, which is unrelated in sequence to APP (15). Low k_{cat} values together with a missing consensus sequence are indicative that conformational dynamics may govern substrate recognition (23). It is generally assumed that proteases cleave their substrates within extended sequences (i.e. β-strands) or loops (24) and most if not all structures of proteases in complex with substrate have corroborated this view. Although protease cleavage sites can actually also reside in α-helices (25,26), cleavable are

mainly those regions which are prone to local unfolding or destabilization (27). Thus, the kinetics of opening of the helix in cleavage domains of the TMD might be the key determinant for substrates. Additionally, local destabilization and length of the membrane anchoring domains at the cytosolic juxtamembrane boundary, as well as β-sheet segments within the extracellular domain of C99 have been reported as important players for γ-secretase cleavage of C99 (28-30). This argues for conformational flexibility of the substrate being a key for productive interactions with the enzyme.

TMD helices are extremely stable due to their hydrogen bond network, which can be loosened by specific residues (31). For instance, substitution of a single leucine by glycine in a membrane spanning poly-L helix facilitates helix bending, enhances local hydration, and triggers a redistribution of α-helical and 3_{10} helical H-bonds (32). The view that global TMD flexibility is required for efficient cleavage of C99 was further supported by biochemical analyses, which showed that mutations introduced at sites that are even far from the cleavage region, can shift cleavage sites as well as cleavage efficiency (33-35). Furthermore, a detailed recent analysis showed that helix-instability of the C99 TMD caused by introduction of helix-destabilizing di-glycine motifs in the cleavage site domain near the ε-sites enhance the initial cleavage and subsequent carboxy-terminal trimming (36). Consistent with this view, biophysical studies indicate that substrate backbone dynamics could play a role in substrate selection (37). In particular the di-glycine hinge region in the C99 TMD (residues G37/G38; Aβ numbering, see **Figure 1A**) has attracted interest over the last years (23,38-40) and has been suggested to provide the necessary flexibility for the interaction with the enzyme (41). Thus, this $G_{37}G_{38}$ motif was shown to coordinate large scale bending movements of the C99 TMD (42) which might allow a putative "swinging-in" of the C-terminal part of the helix to bring the scissile bonds in contact with the active site of γ-secretase (39,43).

In order to evaluate the importance of hinge motions, we designed two artificial mutants of the C99 TMD with the aim to control the amount of hinge bending. A G38L mutation was intended to reduce bending by stabilizing the helix, due to the large hydrophobic side chain of leucine allowing also van der Waals packing with the upstream L34 residue (44), while G38P should conversely increase bending considering the classical helix-breaking potential of proline in soluble proteins (45). If the extent of helix bending around the $G_{37}G_{38}$ hinge determines cleavage by γ-secretase, a decrease in cleavability for the C99 substrate with the G38L mutation and an increase for the G38P mutation, respectively, would be expected. In addition to γ-secretase cleavage assays of recombinant full-length C99 substrates, we assessed the effects introduced by the G38 mutations on structural and dynamical properties of peptides comprising the TMD of C99 and its C-terminal and N-terminal anchors ($C99_{26-55}$, for sequences see **Table 1**) by several biophysical techniques and molecular dynamics simulations. $C99_{26-55}$ peptides were reconstituted in model membranes to investigate the structure/dynamics of the C99 TMD in the hydrophobic environment. In addition, peptides were also studied in trifluoroethanol/water (TFE/H_2O, 80/20 v/v) to mimic the more hydrophilic environment inside γ-secretase (41,42,46-49). TFE/H_2O is a classical solvent mixture to mimic the interior environment of proteins (50,51).

Surprisingly, γ-secretase cleavage of both the G38L and particularly the G38P mutant of C99 was decreased compared to WT, while the structural/dynamical studies of the C99 TMD peptides corroborated the expected "stiffening" and "loosening" effects of the G38L and G38P mutants, respectively, particularly in the TFE/H_2O environment. Furthermore, while the G38L mutant straightened, stiffened and increased helicity of the C99 TMD, the G38P mutant indeed made the helix structurally less defined and more dynamic and introduced a structural kink located at the $G_{37}G_{38}$ sites. However, effects of the G38 mutations on the local dynamical properties of the C99 TMD were observed only in

the vicinity of the $G_{37}G_{38}$ and did not extend to residues around the ε-sites at T48/L49, from which C99 cleavage by γ-secretase is initiated. Nevertheless, in both G38 mutants, the subtle changes in local H-bond flexibility in the vicinity of $G_{37}G_{38}$ introduced large changes of intrinsic bending and twisting dynamics of the helix and distorted sampling of the orientation of the helical turn harboring the ε-sites. We conclude that, (i) altered global motions of the C99 TMD controlled by hinges around $G_{37}G_{38}$ may determine access to the active site, and, (ii) conformational relaxations of the substrate that lead to local helix unwinding required for access to the scissile bond may take place only upon contact of the substrate with the protease.

Results

G38L and G38P glycine hinge mutations in the C99 TMD differently impair γ-secretase-cleavage

To examine whether helix-modulating leucine and proline mutations in the $G_{37}G_{38}$ hinge in the TMD of C99 have the expected impact on the cleavage by γ-secretase, G38L and G38P mutants of the C99-based recombinant substrate C100-His_6 (52) were purified and used to assess their cleavability in an established *in vitro* assay using detergent-solubilized HEK293 membrane fractions enriched for γ-secretase (53). To confirm cleavage specificity, γ-secretase inhibitor L-685,458 (54) was included in control samples.

As expected, Aβ and AICD levels of the G38L mutant were reduced (~47% and ~38%, respectively) compared to WT (**Figures 1B, C, D** and **E**). However, in contrast to our initial assumption, cleavage of the G38P mutant was even more reduced, leading to a residual Aβ and AICD production of ~16 % and ~8 %, respectively, compared to the WT. Thus, the hinge region is a critical part of the APP TMD, which, when mutated, can strongly influence substrate cleavability by γ-secretase. To also investigate the impact of the

mutations on the carboxy-terminal trimming activity of γ-secretase, i.e. its processivity, we analyzed the finally released Aβ species with MALDI-TOF mass spectrometry (MS) (**Figures 1F**). Strikingly, while Aβ40 was as expected the predominant species for the cleavage of the WT substrate, Aβ37 was the major cleavage product for the G38L mutant. Thus, although the initial ε-cleavage was impaired for the G38L mutant, its processivity was enhanced. In contrast, as in the case for WT, Aβ40 remained the major cleavage product for the G38P mutant, for this mutant no species shorter than Aβ39 were detected. Thus, for both mutant substrates ε-cleavage and processivity by γ-secretase were markedly affected.

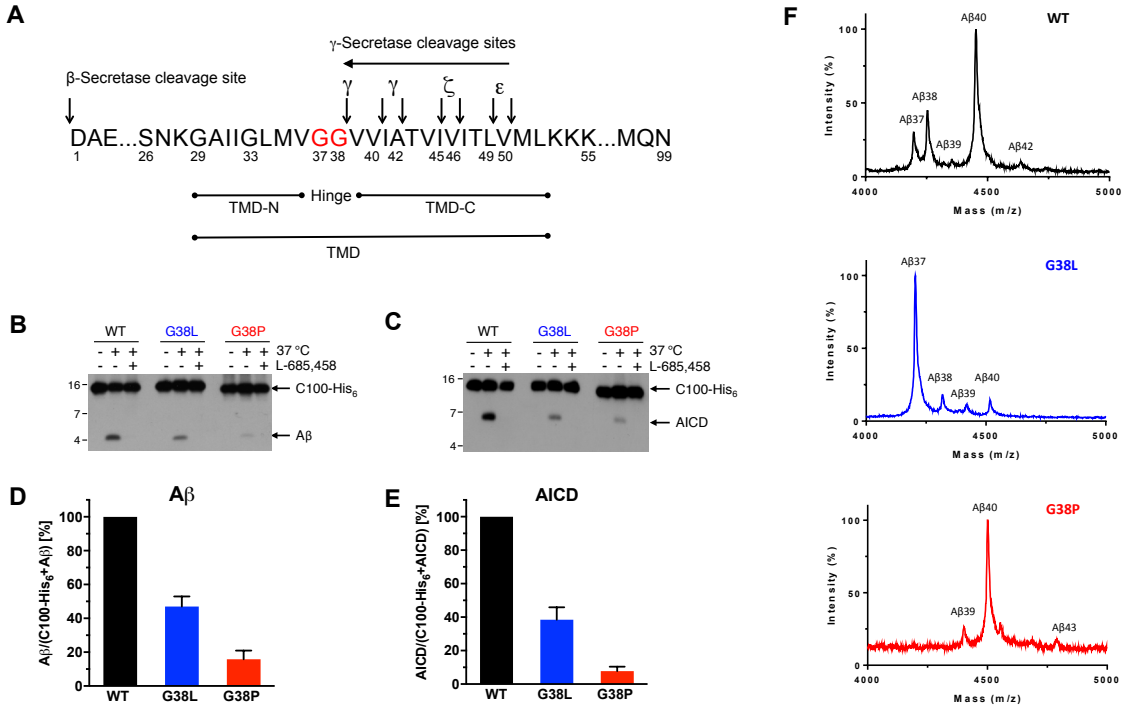

Figure 1. C99 G38P and G38L mutants differently impair γ-secretase cleavage.

(A) Primary structure of C99 (Aβ numbering) and its major γ-secretase cleavage sites. **(B)** Levels of Aβ and **(C)** AICD were analyzed by immunoblotting after incubation of the purified C100-His_6 WT and mutant constructs with detergent-solubilized HEK293 membrane fractions at 37°C. As controls, samples were incubated at 4°C or at 37°C in the presence of γ-secretase inhibitor L-685,458. **(D)** Quantification of Aβ and **(E)** AICD levels. Values are shown as percent of WT, which was set to 100%. Data are represented as mean

± S.E.M. (n = 3, each n represents the mean of 3 technical replicates). **(F)** Mass spectroscopy analysis reveals that relative amounts of produced Aβ species were dramatically altered for G38L and G38P mutant substrates compared to WT.

G38 hinge mutations cause structural changes of the C99 TMD helix

To understand why both hinge mutations impair γ-secretase cleavage, we next investigated how the G38 mutations might impact on structural and dynamical properties of the C99 TMD. To compare the effects of the G38L and G38P mutants on the helical conformation of the C99 TMD, WT and mutant peptides $C99_{26-55}$ peptides (for sequences see Methods, **Table 1**), were incorporated into large unilamellar vesicles composed of POPC. As shown in **Figure 2A**, CD spectroscopy measurements demonstrated that the peptides contain a high content of α-helical conformation in the lipid bilayer. As expected, the helical conformation was stabilized for the G38L (indicated by the more negative ellipticity at 220 nm) and destabilized for the G38P mutant. Similar effects were found when the peptides were analyzed in TFE/H_2O (80/20 v/v) (**Figure 2B**). In this solvent, ellipticity and the shape of the spectra was different compared to POPC, which was due to the different solvent properties, but the minima at 208 and 220 nm were nevertheless indicative of a high degree of helicity. The latter was corroborated by solution NMR (**Figure 2C,** see **Figure S1** for complete data set). Structural information was derived from NOE patterns and secondary chemical shifts (Δδ). Over the entire TMD sequence, $C99_{26-55}$ WT showed cross peaks that are typical for an ideal α-helix (containing 3.6 residues per turn, **Figure S1**). Analysis of secondary chemical shifts ($\Delta\delta(^{13}C_\alpha)$, $\Delta\delta(^{1}H_\alpha)$, and $\Delta\delta(^{13}C_\beta)$) (**Figure 2C, Figure S1**) allowed a more detailed view on helical stability. $\Delta\delta(^{13}C_\alpha)$ and $\Delta\delta(^{1}H_\alpha)$ in particular, as well as $\Delta\delta(^{13}C_\beta)$, indicated a strong helicity for a C-terminal domain (TMD-C) ranging from V39 to L52. In contrast, the N-terminal domain (TMD-N), ranging from S26 up to V36, seemed to form a less stable helix. At positions G37 and G38 the helical pattern appeared to be

disturbed which is obvious from the reduced values $\Delta\delta(^1H_\alpha)$ at these residues. This observed pattern of TMD-N and TMD-C domains flanking the short $G_{37}G_{38}$ segment of lower stability is consistent with previous results (41,42,48,55).

With regard to the G38 mutants, no major changes in the NOE patterns and secondary chemical shifts were observed. However, a detailed view showed small differences in secondary chemical shifts both for G38L and G38P. G38L appeared slightly stabilized compared to the WT. ^{13}C chemical shift changes were restricted to the two helical turns around L38 (M35 - I41) and the immediate termini (**Figure 2D**). The high number of differences in both $\Delta\delta(^{13}C_\alpha)$ and $\Delta\delta(^1H_\alpha)$ shifts of G38P compared to those of the WT values (**Figure 2E**) indicated changes in structure or stability induced by the mutation that, however, were too subtle to also result in altered NOE patterns. This stems from the fact that for dynamic helices NOEs are dominated by the most stable conformation, whereas the highly sensitive chemical shifts are affected even by minuscule changes. Particularly the helicity of the N-terminal part up to V36 had decreased according to the chemical shift pattern, as predicted, but also the remaining C-terminal part showed significant and irregular deviations compared to the WT. Concomitantly, we observed an overall increase of H_N resonance line widths, which is indicative of a global conformational exchange (**Figure S2**). Also several minor alternative conformations were visible, that resulted in more than one H_N/H_α resonance for many residues (up to four for some residues) (**Figure S2**). Taken together, consistent with the CD data, the solution NMR data show that the $C99_{26\text{-}55}$ peptide has a high propensity to form a helical structure, which is only slightly reduced in the $G_{37}G_{38}$ hinge region. Interestingly, the TMD-C, i.e. the region in which the cleavages by γ-secretase occur, has a much stronger helicity compared to the TMD-N. The G38L mutation caused a stabilization of the helix around the $G_{37}G_{38}$ hinge, albeit small, whereas the G38P mutation disturbed the WT helix both in the TMD-N and TMD-C parts relative to the $G_{37}G_{38}$ residues.

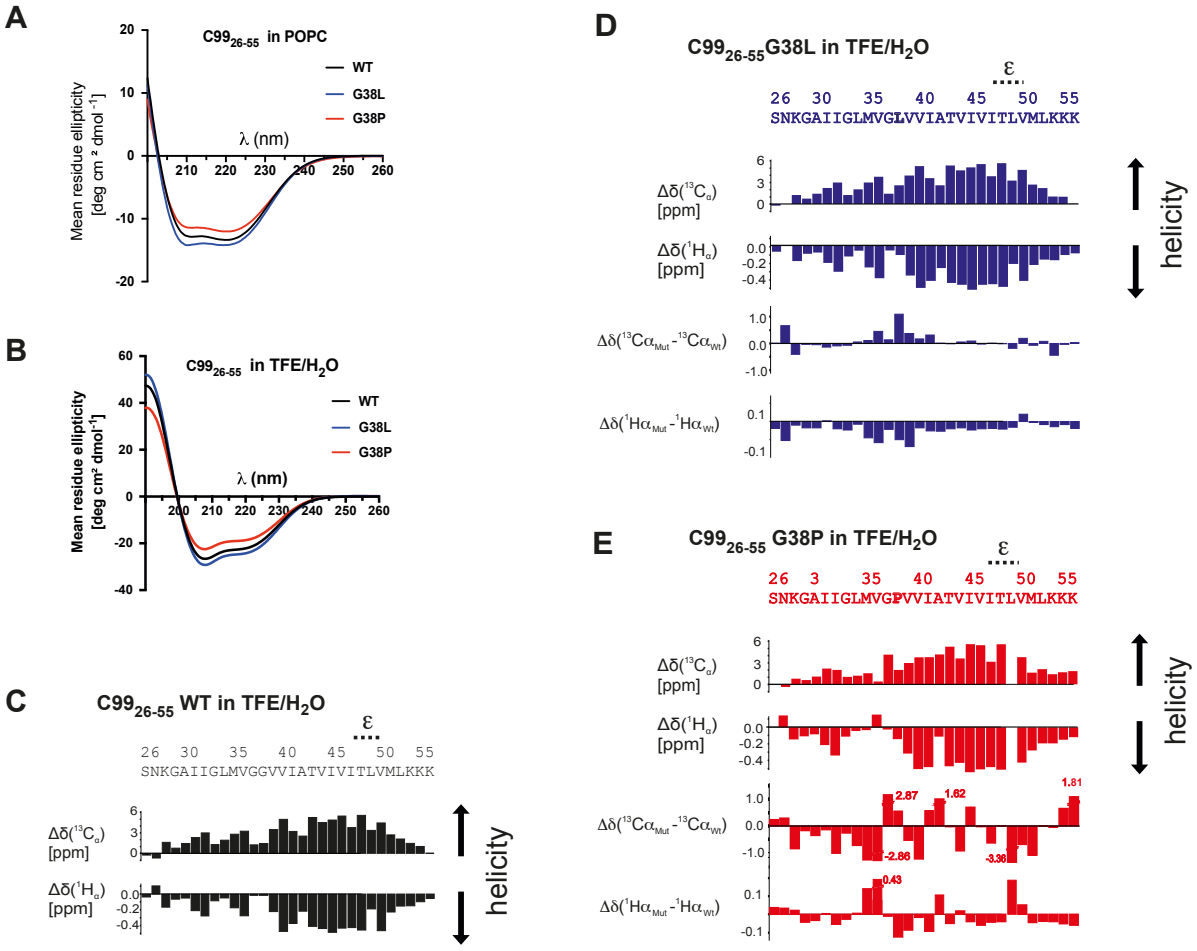

Figure 2. Helicity of $C99_{26-55}$ TMD peptides is increased by the G38L and distorted by the G38P mutation. (**A**) CD spectra of $C99_{26-55}$ WT, G38L and G38P mutant peptides reconstituted in POPC model membranes and **(B)** dissolved in TFE/H_2O. Compared to WT, helicity is slightly increased for the G38L mutant, and decreased for G38P. (**C**) Solution NMR of $C99_{26-55}$ WT, G38L **(D),** and G38P **(E)** mutants in TFE/H_2O. Chemical shift indices (Δδ) for $^{13}C_\alpha$, and $^{1}H_\alpha$ atoms of each residue, and differences between Δδ values of mutant and WT reveal a high degree of helicity, especially in the TMD-C, which is distorted for the G38P mutant.

G38 mutant helices display altered flexibility and hydrogen-bond occupancies around the $G_{37}G_{38}$ hinge

We next assessed the conformational flexibility of the $C99_{26-55}$ WT and mutant helices, as expressed by intrahelical amide H-bond stabilities. To this end, we performed backbone amide deuterium-to-hydrogen (D/H) exchange experiments in TFE/H_2O using MS (MS-DHX) as well as hydrogen-to-deuterium (H/D) exchange using NMR (NMR-HDX). Determining amide exchange in POPC membranes was not practical, as the bilayer effectively shields central parts of the TMD helix (56,57) so that backbone amides engaged in H-bonds do not exchange. Thus, the reduced stability of backbone amide H-bonds associated with more flexible helices results in faster amide exchange. Exchange rate constants also depend on the local concentration of hydroxyl ions, the exchange catalyst. The rate constant of the underlying chemical charge transfer step is influenced by side-chain chemistry (58). **Figure 3A** shows the result of MS-DHX experiments of >98% deuterated $C99_{26-55}$ WT and mutant peptides diluted into TFE/H_2O at a peptide concentration of 5 µM, at which the helices remain monomeric (41). Consistent with previous results (41,42,47,59), overall D/H exchange is characterized by rapid deuteron exchange within minutes followed by a relatively fast exchange over 60 min (**Figure 3A,** inset) and a subsequent very slow process; near complete exchange is seen after three days. Relative to WT, the G38L mutation slowed hydrogen exchange. G38P results in a slightly faster exchange. As part of the lower deuterium content in G38P results from the lack of one amide deuteron at the cyclic side chain of proline, we also detect a reproducible decrease of a further 0.5 D after a few minutes of exchange (**Figure 3A,** inset) suggesting acceleration of exchange by the mutation. To obtain insight into local amide H-bond strength, we next measured residue-specific amide D/H exchange rate constants ($k_{exp,DHX}$) using electron transfer dissociation of our TMD peptides in the gas-phase after various periods of exchange (MS-ETD-DHX) (32,37). In order to enhance fragmentation efficiency, we substituted the N-terminal SNK

sequence of the $C99_{26-55}$ TMD by KKK. As shown in **Figure 3B,** for all three peptides, D/H-exchange occurred within minutes for residues up to M35 within TMD-N and at the C-terminal KKK residues (60). The rate constants gradually decreased by up to two orders of magnitude in the region harboring the $G_{37}G_{38}$ motif. Interestingly, compared to WT, both G38 mutants perturbed exchange downstream of the mutation site in the region around the γ-40 cleavage site. While the G38L mutation decreased $k_{exp,DHX}$ significantly between V39 and T43, G38P increased $k_{exp,DHX}$ mainly for V39 and V40. Very slow exchange was observed in TMD-C, containing the ε-cleavage sites, which was not affected by the G38 mutants.

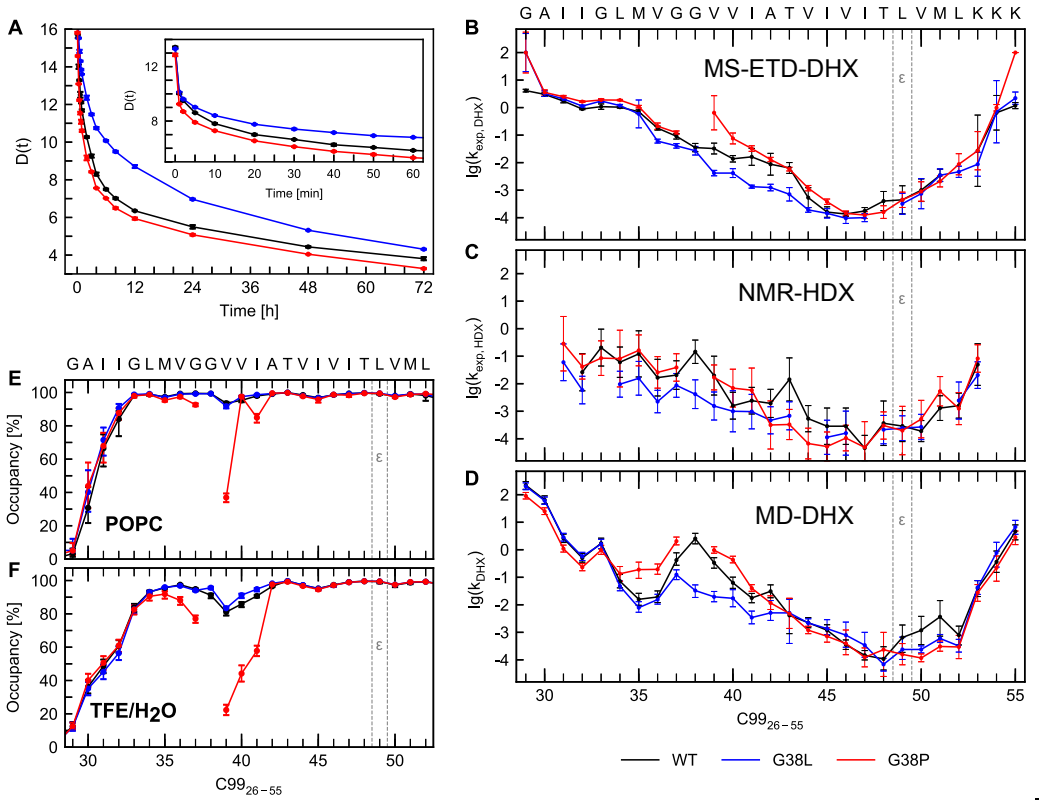

Figure 3. Deuterium-hydrogen exchange rates along the TMD of $C99_{26-55}$ to gauge backbone H-bond stability reveal an impact of the G38 mutations around the mutated positions, but not at the ε-cleavage sites. (A) Overall DHX kinetics of $C99_{26-55}$ WT, G38L and G38P mutant peptides measured with MS-DHX. Complete deuteration is followed by back-exchange in TFE/H_2O, pH 5.0, T = 20°. Exchange kinetics during the first 72 h and 60

min (inset) (n = 3, error bars showing SD are smaller than the size of the symbols) were measured. **(B)** Site specific D/H exchange rate constants ($k_{exp,DHX}$ [min^{-1}]) of $C99_{26-55}$ WT, G38L and G38P mutants dissolved in TFE/H_2O as determined by MS-ETD (error bars show 95% confidence intervals). **(C)** Site specific H/D exchange rate constants ($k_{exp,HDX}$ [min^{-1}]) determined by NMR. (n = 3, error bars show SD). (**D**) Site-specific k_{DHX} [min^{-1}] as computed from MD simulations (error bars show 95% confidence intervals). **(E)** Backbone H-bond occupancy of the individual residues of $C99_{26-55}$ WT and its G38L and G38P mutants in POPC and **(F)** in TFE/H_2O revealed by MD simulations.

Additionally, we measured H/D exchange by NMR spectroscopy (note that H/D and D/H exchange kinetics are expected to differ only by a constant factor reflecting the 80% slower chemical exchange from a protiated amide as compared to a deuterated one (60). The shape of the NMR-HDX profile (**Figure 3C**) roughly matches the MS-ETD-DHX profile in that exchange within the TMD-N is faster than within TMD-C (**Figure 3B**). Further, NMR confirms locally reduced exchange rates for the G38L mutant and locally enhanced rates for G38P, although the experimental errors prevent clear assignments of the differences to individual residues. Again, the amides of both ε-site residues are not affected by the mutations. The generally lower H/D rate constants, relative to the respective DHX values, are ascribed to the intrinsically slower chemical H/D exchange as compared to D/H exchange (61).

The D/H exchange experiments were complemented by MD simulations. DHX rate constants reconstructed from the fraction of open H-bonds and the local water concentration, as obtained from the simulations, could reproduce well the overall MS-DHX kinetics ($0.400 \leq \chi^2 \leq 1.493$, **Figure S3**). In accordance with the ETD-derived rate profile, the simulated residue specific k_{DHX} profiles (**Figure 3D**) revealed fast exchange at both termini and very slow exchange in TMD-C. Additionally, the slow exchange at the ε-sites, without

significant differences between WT and the G38 mutants was confirmed. Taken together, for all peptides, local amide exchange rates determined by three different techniques consistently report perturbed backbone stability in the helix-turn downstream to the G38 mutation site in the γ-cleavage site region, but no alterations in helix stability around the ε-cleavage sites.

To gain further insight in the distribution of flexibility along the $C99_{26-55}$ peptides we focused on the site-specific population of intrahelical H-bonds. Membrane proteins can show backbone H-bond shifting that does not induce permanent conversion to alternative helical forms (e.g. 3_{10} helix) but rather confers flexibility to the TMD helices and provides pathways for conformational changes like helix bending and twisting that accompany functional cycles (31). Switching between α and 3_{10} H-bonds has been detected previously for $C99_{28-55}$ (41,42,48) as well as for other TMDs (30,32). We calculated both, α– and 3_{10}-helical H-bond occupancies from the MD simulations (**Figure S4**) and report the combined occupancies where an amide is counted as protected if either the α or the 3_{10} H-bond is formed in **Figures 3 E** and **F**. For the WT and G38L peptides in POPC a 10% drop of occupancy of i,i-4 H-bonds emanating from backbone amides of V_{39} and V_{40} was largely compensated by formation of 3_{10} H-bonds (**Figure S4**). The resulting occupancy loss for these H-bonds (**Figure 3E**) correlates with flexibility at the $G_{37}G_{38}$-hinge where H-bonds on the opposite face of the hinge have to stretch in order to allow for bending. In TFE/H_2O the whole stretch of H-bonds spanning from the G_{33} carbonyl-oxygen to the amide-hydrogen at I_{41} was destabilized. Here, a maximal drop in α-helicity by 40% was only partially compensated by formation of 3_{10} H-bonds (**Figure S4**) indicating enhanced conformational variability.

In the TMD-C of all $C99_{26-55}$ peptides both in POPC and TFE/H_2O, we found an ~5-10% population of 3_{10}-H-bonds around the amides of T43/V44 and T48/L49. However, neither shifting between α and 3_{10} H-bonds nor helix distortions involving the carbonyl-

oxygen at the ε-sites or other signs of helix distortions could be detected for the G38 mutants (**Figures S4** and **3E, F**). Remarkably, the occupancies of 3_{10} H-bonds did not change when changing solvent from POPC to the hydrophilic environment in the TFE/water solution. This showed, that the ε-sites were in a rather stable helical conformation, which was not perturbed by the G38 mutations.

G38 mutants do not change the tilt of the C99 TMD helix in a POPC bilayer but alter the orientation of the ε-cleavage sites region

In addition to local variations of the structure and stability of the C99 TMD investigated above, it is possible that also global orientation of the TMD helix in the bilayer plays an important role in substrate recognition and cleavage. TMD helices usually do not align perfectly with the normal of a phospholipid bilayer, but tilt in order to compensate hydrophobic mismatching between the length of the hydrophobic domain of the TMD and the hydrophobic thickness of the lipid bilayer (62). Tilt angles fluctuate with time. Additionally, azimuthal rotations of the tilted helix along its axis are not randomly distributed reflecting preferential side chain interactions with the individual components of the phospholipid bilayer (63-65). To explore a potential influence of the G38 mutations on these properties, we investigated the distribution of tilt (τ) and concomitant azimuthal rotation (ρ) angles **(Figure S5)** of $C99_{26\text{-}55}$ embedded in a POPC bilayer by solid-state NMR (ssNMR) and MD simulations. First, proper reconstitution of the $C99_{26\text{-}55}$ WT and G38 mutant peptides as helices into the POPC membranes for solid state NMR was confirmed by analysis of the chemical shifts of the C_α peaks of A30 in the ^{13}C spectra (**Figure S6**). Next, the C_α-H_α order parameters of residues A30, G33 (only for WT), L34, M35 (only for WT), V36 (only for WT), G37, A42 (only for WT) and V46 of $C99_{26\text{-}55,}$ chosen to represent the helical wheel with C_α-H_α bond vectors pointing in many different directions, were measured by ssNMR. For G38 mutant peptides only A30, L34, G37 and V46 were measured as

compromise between expensive labeling and highest information impact to be expected. In order to estimate τ and ρ of the TMD helix in $C99_{26-55}$, the GALA model (66) was used (see Materials & Methods).

In **Figure 4A** the normalized inverse of the root-mean-square deviation ($RMSD_{Norm}$) between data and model is shown as function of tilt and azimuthal rotation angles. In the ssNMR experiments, for all three peptides relatively broad τ, ρ landscapes with several possible orientations were found. For all three peptides reliable helix orientations were found comprising helix tilt angles τ on the order of 30° or below. For these solutions the azimuthal angle ρ usually is not well defined which is not surprising since ρ becomes meaningless for small tilt angles. An averagely small tilt angle for C99 TMD of was also found by others (67), although in the latter study a very heterogeneous picture with different orientation and dynamics of several helix parts was concluded.

As shown by the probability distributions of (τ,ρ) combinations (**Figure 4B**), the results from MD simulations are in agreement with the ssNMR observations. Thus, average tilt angles calculated from the simulations are in the order of 30° or below (WT: 23.1° with 95% CI [20.2, 26.2] in agreement with others (38), G38L: 21.8° ([18.7°, 25.2°]) and G38P 25.9° ([22.2°, 29.9°]). A precise ρ angle could not be calculated from the order parameters obtained from ssNMR, but only a range of possible orientations. Given the similar broad distribution of ρ angles obtained from the MD simulation (**Figure 4B**), one apparently has to take into account the high dynamics of the TMD helices in the liquid-crystalline membranes. This is likely a characteristic feature of these segments under biological conditions, which prevents accurate measurement of the ρ parameter. In the same way, average values for ρ computed from the MD simulations would be statistically meaningless. We conclude that the TMD helices are highly dynamic in POPC membranes and that there are no significant differences in the tilt angles of WT and G38 mutants. However, compared to WT, broader (τ, ρ) distributions are for G38P and narrower distributions for G38L, as found in the MD

simulations, might indicate differences between these mutants in the intrinsic topology of peptide flexibility including the flexibility in the hinge region.

With respect to the reduced cleavability of the G38 mutants, the orientation of the ε-sites, at which the substrate is cleaved first, is of special interest. We describe the orientation of the helical turn carrying the ε-cleavage sites (domain B: I47-M51, colored blue in **Figures 4 D/E**) with respect to the orientation of the helical turn in TMD-N around G_{33} (domain A: I31-M35, colored red in **Figures 4 D/E**) by a pair of angles (see **Figure S5B**). The bending angle (θ) is calculated as the angle between the axes through the two segments. The swivel angle (ϕ) is defined by the rotation of the domain B vector in the plane perpendicular to the domain A vector relative to a zeropoint set at the C_α of G_{33} (ϕ=0°) when viewed along the helix from the N-terminus. We analyzed the bend and swivel conformational sampling for the $C99_{26-55}$ WT and G38 mutant peptides in POPC and TFE/H_2O and report probability distributions of (θ,ϕ) combinations in **Figure 4C** as well as average bend/swivel geometries in **Table S1.** Representative conformations determined by K-means clustering of (θ,ϕ) combinations are exemplified in **Figures 4D** and **4E**.

Generally, we observe an asymmetry of the bend-swivel behavior of the ε-site orientations in all peptides with respect to both, structure and dynamics. In POPC, ε-sites of the WT and G38L peptides exhibit bending rarely exceeding 30° with a mean values of ~12°. For the G38P mutant, an increased population of conformations with θ even larger than 40°, lack of conformations with θ<15° (**Figure 4F**), and an average bending of ~32° reveal a persistent reorientation of the ε-sites toward the N-terminal segment. However, the range of bending angles sampled around the mean value is ~30° for WT as well as for mutant peptides. Examination of the swivel angles reveals anisotropic bending, where the preference for particular regions of the swivel space depends on the residue at the 38 positions. Both G38 mutations impart a counterclockwise shift of the sampled swivel angle space. As a consequence, the mean ϕ angle shifts by 10° for the G38L mutant and by 40° for

the G38P mutant with respect to the WT (**Table S1**). Compared to WT and G38L peptides, which sample a swivel angle range of ~100°, the G38P mutation favors a much narrower range of swivel angles (~60°). Changing from the POPC membrane to TFE/H_2O does not shift preference of the peptides for the particular regions in the swivel space (**Figure 4C**). However, we note generally an increase in the fraction of conformations with larger bending angles (**Figure 4F**). In the case of the G38P peptide, we even notice excursions to a population with unreasonably large bending angles θ>80° around the $G_{37}P_{38}$ sites (**Figure 4E**).

Taken together, the comparison of the bend/swivel behavior of ε-site orientations revealed an asymmetry in helical conformations (**Figure 4E**). The G38P mutation alters both bend and swivel angles, i.e. vertical and horizontal position of the ε-cleavage site region. In contrast, the G38L mutation mainly impacts the swivel angles and thus misdirects the ε-cleavage region horizontally.

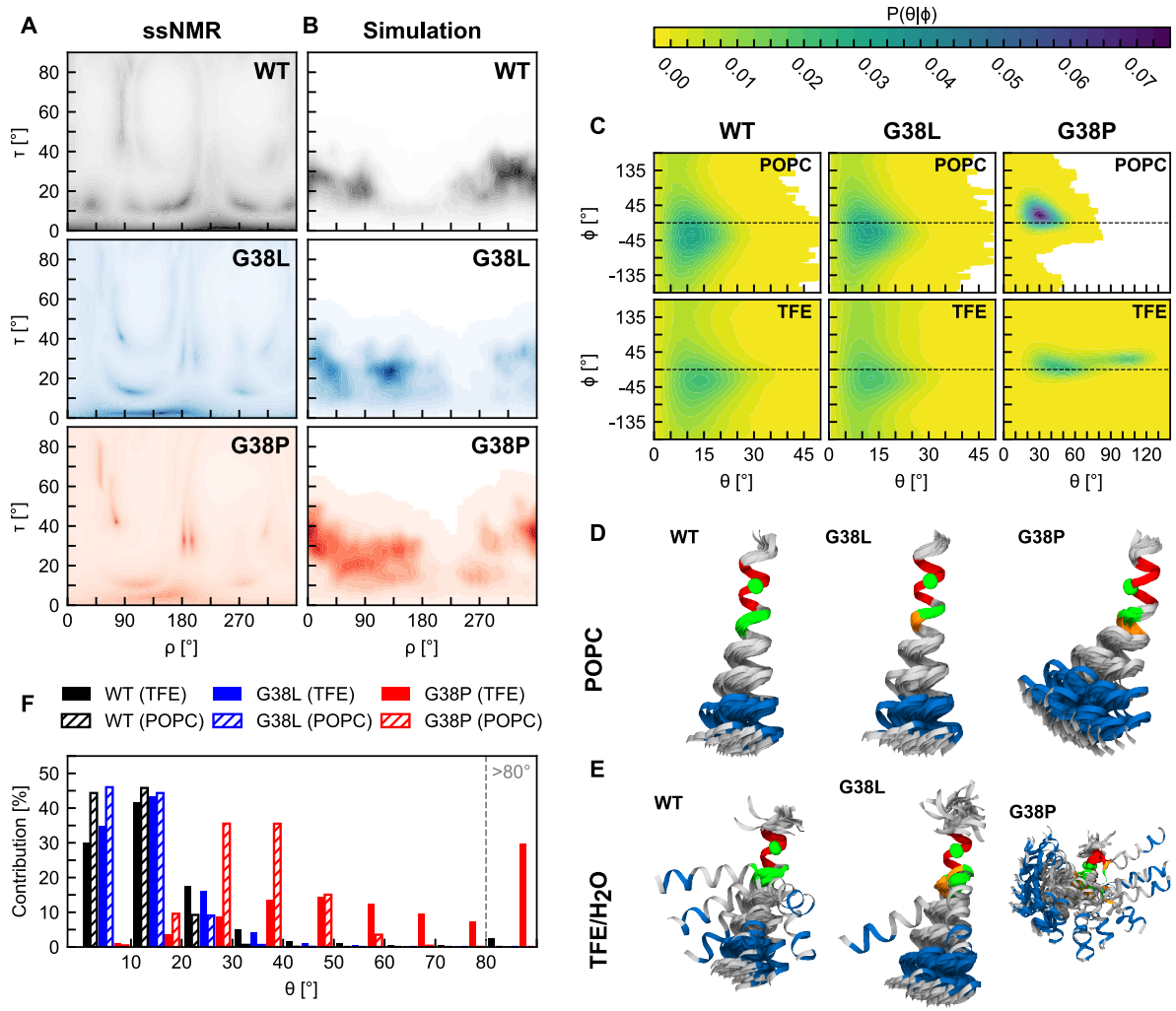

Figure 4. G38 mutations of the C99$_{26-55}$ peptide do not significantly alter its membrane orientation but impact orientation of the ε-cleavage sites region **(A)** Heat maps of $RMSD_{Norm}$ values for tilt (τ) and azimuthal rotation (ρ) angle combinations of C99$_{26-55}$ WT, G38L and G38P mutant peptides in a POPC bilayer as determined by ssNMR. Dark areas represent angle combinations for the best solutions. The plot of the WT is based on more C_α-H_α order parameters since more labels were available for this peptide. (**B**) Probability distributions P(τ,ρ) of τ and ρ angle combinations from MD simulations. Dark areas represent high probabilities. (**C**) Probability distributions of bending (θ) and swivel (ϕ) angle combinations characterizing the orientation of ε-cleavage sites in WT, G38L and G38P mutants in POPC and in TFE/H_2O, calculated from MD simulations. (**D**, **E**) Visualization of

representative conformations for WT and G38 mutants in **(D)** POPC and **(E)** TFE/H_2O. Domains colored in blue indicate the TMD-C segment I47-M51 carrying the ε-sites. Domains colored in red represent the TMD-N segment I31-M35, which was also used to overlay the structures. The $G_{37}G_{38}$ motif is colored in green. For the G38 mutants the L and P residues are depicted in orange. Green spheres represent the C_α atom of G33 used as reference for the determination of swivel angles. A swivel angle of $\phi = 0°$ indicates bending of the TMD-C segment I47-M51 in the direction of G_{33}. Positive ϕ-angles count counter-clockwise rotation. (**F**) Distribution of conformations according to their bending angles θ. The last class summarizes all conformations with $\theta > 80°$.

G38 mutations relocate hinge sites and alter extent of hinge bending and twisting

The results discussed so far revealed that the impact of the $G_{37}G_{38}$-hinge mutations on H-bond stability is confined to a small number of residues in the hinge region. Although H-bonding around the ε-sites was not altered, we noticed that sampling of ε-site orientations is distorted in the mutants. Generally, TMD helices bend and twist by changing the direction of the helix axis or the helical pitch around various flexible sites (68-71). All these helix distortions contribute to the variability of the orientation ε-cleavage site region (**Figure 4C**). Here we consider the fundamental types of helix motions describing bending or twisting around a single hinge (referred to as types B and T) and combined bending and/or twisting around a pair of hinges (referred to as types BB, BT, TB and TT) (32,48). These six types of subdomain motions are exemplified in **Figure 5A** for the $C99_{26\text{-}55}$ WT TMD helix. Interestingly, among the monomeric structures of the 10 mammalian single-span TMDs proteins listed in the PDB (protein data Bank, https://www.rcsb.org)), deformations associated with a pair of hinges are observed for two of them (the integrin receptor and integrin α1), while five of them, including the APP TMD, bend near the center of the helix (68).

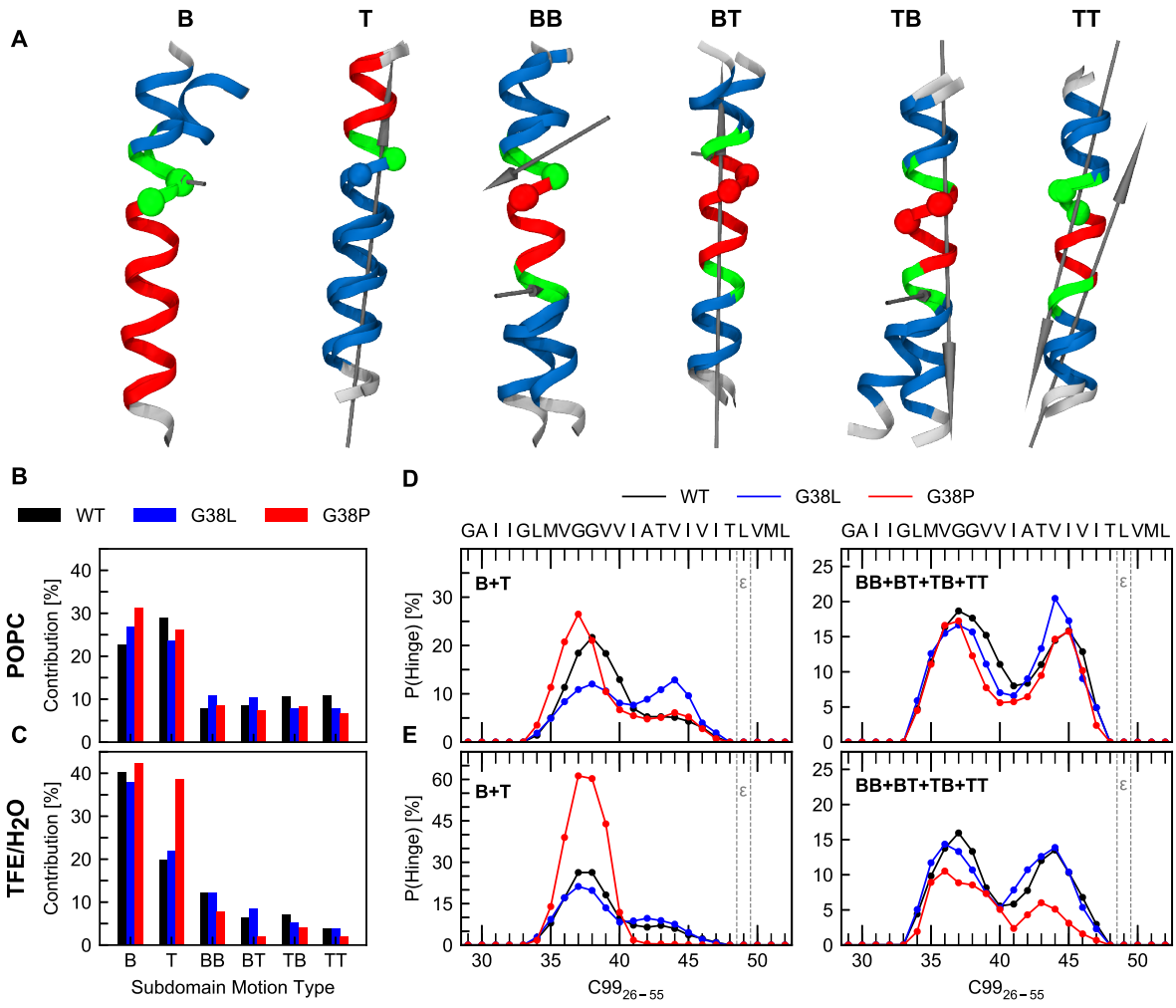

Figure 5. G38 mutations alter global bending and twisting motions. (**A**) The fundamental motions of helices exemplified for the $C99_{26\text{-}55}$ WT peptide. Motion types are bending (B) and twisting (T) coordinated by a single hinge as well as combinations of bending and twisting (types BB, BT, TB, TT) coordinated by a pair of hinges. Helical segments moving as quasi-rigid domains are colored in blue and red. Residues, which act as flexible hinges are colored in green. Spheres represent C_α atoms of G37 and G38 and are colored according to the domain in which they are located. Screw axes passing the hinge regions are shown in grey. A screw axis perpendicular to the helix axis indicates a bending-like motion while a screw axis parallel to the helix axis indicates a twisting-like motion. For mixed bending/twisting motions, a larger projection of the screw axis with respect to the

helix axis indicates a higher percentage of twisting. In addition to the central $G_{37}G_{38}$ motif, a flexible region around $T_{43}VI_{45}$ provides hinge flexibility within the TMD-C as detailed in **(D)** and **(E)**. (**B**) Probability of all 6 types of hinge bending and twisting motions in POPC and (**C**) TFE/H_2O. (**D, E**) Probability by which a residue is identified as a hinge site in the single-hinge (B+T) and double-hinge motions (BB+BT+TB+TT) for peptides in POPC (**D**) and (**E**) TFE/H_2O.

In order to understand the impact of the G38 mutations on the variability of the orientations of the ε-cleavage site region, we investigated the subdomain motions in WT and mutant peptides. Hinge sites are detected as flexible joints able to coordinate the motion of more rigid flanking segments (32,48,60,72). The contribution of each type of subdomain motion is depicted in **Figures 5B** and **C**. More than 90% of the sampled conformations deviated from a straight helix. In the POPC bilayer, motions around a single hinge (types B+T) contributed ~55% to overall backbone flexibility, the double-hinge motions in sum contributed ~35%. Note that the helices do not only bend around the $G_{37}G_{38}$ hinge but populate also a large fraction of twisted conformation (type T, 25-30%). The loss of packing constraints from lipids as well as enhanced H-bond flexibility (**Figures 3E, F**) in TFE/H_2O correlated with favored helix bending (types B and BB) in WT and G38L, but enhanced twisting (type T) and almost complete loss of double-hinge motions in G38P.

Due to their reduced H-bond stabilities, combined with extensive shifting between α- and 3_{10} H-bonding (**Figure S4**), and the absence of steric constraints, the $V_{36}GGV_{39}$ sites in the C99 TMD are optimally suited to act as hinges, an observation discussed already previously (38,40,42,48,55). A second hinge located upstream to the ε-sites around residues $T_{43}VI_{45}$ was only recently discussed in relation to the impact of FAD mutations in the cleavage domain of the C99 TMD (48). When acting in combination (motion types BB, BT,

TB, TT), both hinges correlate bending/twisting of the flanks at the C-terminus (residues I47-M51) and the N-terminus (residues I31-M35) with respect to the middle helix (residues V36-V46). The impact of the G38 mutations on local H-bond flexibility (**Figure S4**) alters also the location of flexible joints coordinating the motions of the flanking segments (**Figures 5 D** and **E**). In POPC, hinge propensities clearly shifted from G38 in the WT to G37 for G38P. The shift of a hinge site by one residue correlates with the counter-clockwise reorientation of the ε-sites as documented also in **Figure 4C** by a shift of the swivel angle distribution towards more positive values (see also **Table S1)**. The most severe impact on single-hinge location was noticed for the G38L mutant in POPC. Restricted rotational freedom around the L38 in the tightly packed lipid environment eliminates preference for single-hinge bending and twisting around the $G_{37}G_{38}$ hinge and enhances bending around the second $T_{43}VI_{45}$ hinge. Most importantly, although WT and G38L peptides sample similar regions in the bend/swivel space of ε-site orientations (**Figure 4C**), the backbone conformations contributing to the orientation variability are different. In TFE/H_2O (**Figure 5E**), anisotropic bending over the $G_{37}G_{38}$ hinge was confirmed by the equal hinge propensity of these two residues in the WT peptide, while both mutants slightly preferred G37.

In conclusion, the simulations show that the heterogeneous distribution of flexibility in the C99 TMD provides several hinge regions coordinating bending and twisting motions. The helix deformations associated with these motions and the location of the hinges are determined by sequence (WT vs. G38L or G38P) as well as by packing constraints imposed by the environment (POPC membrane vs. TFE/H_2O). Thus, hinge motions are favored by the absence of steric constraints as well as by flexible H-bonds shifting between i+3 and i+4 partners. Although the ε-cleavage sites keep their stable helical structure, they gain mobility due to a variety of backbone motions around two flexible regions acting as hinges, the $V_{36}GGV_{39}$ region and the $T_{43}VI_{45}$ region.

G38 mutants do not alter contact probabilities with γ-secretase

Since the G38 mutations are localized close to potential TMD-TMD interaction interfaces (i.e. $G_{29}XXXG_{33}$, $G_{33}XXXG_{37}$ and $G_{38}XXXA_{42}$ motifs (38,41)), an alternative rationale for the impaired γ-secretase cleavage of the G38 mutants (**Figure 1**) could be altered contact preferences with γ-secretase. To screen for contact interfaces of the C99 TMDs with γ-secretase, we set up an *in silico* docking assay for transmembrane components (DAFT, (73)) using a coarse-grained description of POPC lipids, water, substrate TMD and γ-secretase. This protocol was previously shown to reliably reproduce experimentally verified protein-protein interactions in a membrane (73,74). The use of >750 replicas per TMD starting from unbiased non-interacting initial states, sampling for at least 1 μs per replicate and inclusion of low-amplitude backbone dynamics of γ-secretase (75) provided exhaustive sampling of potential contact sites and exceeds previous assessments of C99 binding sites with respect to both number of replicates and simulation time (59,76).

Our calculations show that the TMDs of WT and both mutants could principally interact with the surface of the γ-secretase complex and contact all four complex components **(Figure 6A)**. Interestingly, in agreement with previous substrate-crosslinking experiments (21), the WT C99 TMD showed the highest binding preference for the PS1 NTF (**Figure 6A**). The normalized C99 TMD proximities for each residue of γ-secretase (**Figure 6B**) revealed that contacts with the highest probabilities were formed between the juxtamembrane $S_{26}NK_{28}$ residues of C99 and the two threonine residues T119 and T124 in the hydrophilic loop 1 between TMD1 and TMD2 of PS1. This observation indicates that the presenilin TMD2 may represent a major exosite of γ-secretase. Interactions between PS1 TMD2 and the C99 TMD could mainly be attributed to contacts of the G33, G37 and V40 of the C99 TMD with residues A129, I133 and A136 of PS1 TMD2 (**Figure 6C**). Additional contact sites of the C99 TMD at V44 and I47 are located on the same face of the

C99 TMD helix as the main contact sites (**Figure 6C**). However, the probabilities of the observed contacts with the enzyme were not altered by the G38 mutations. Thus, based on our substrate docking simulations, the structural alterations of the C99 G38 mutant TMD helices may not cause gross alterations in initial substrate-enzyme interactions.

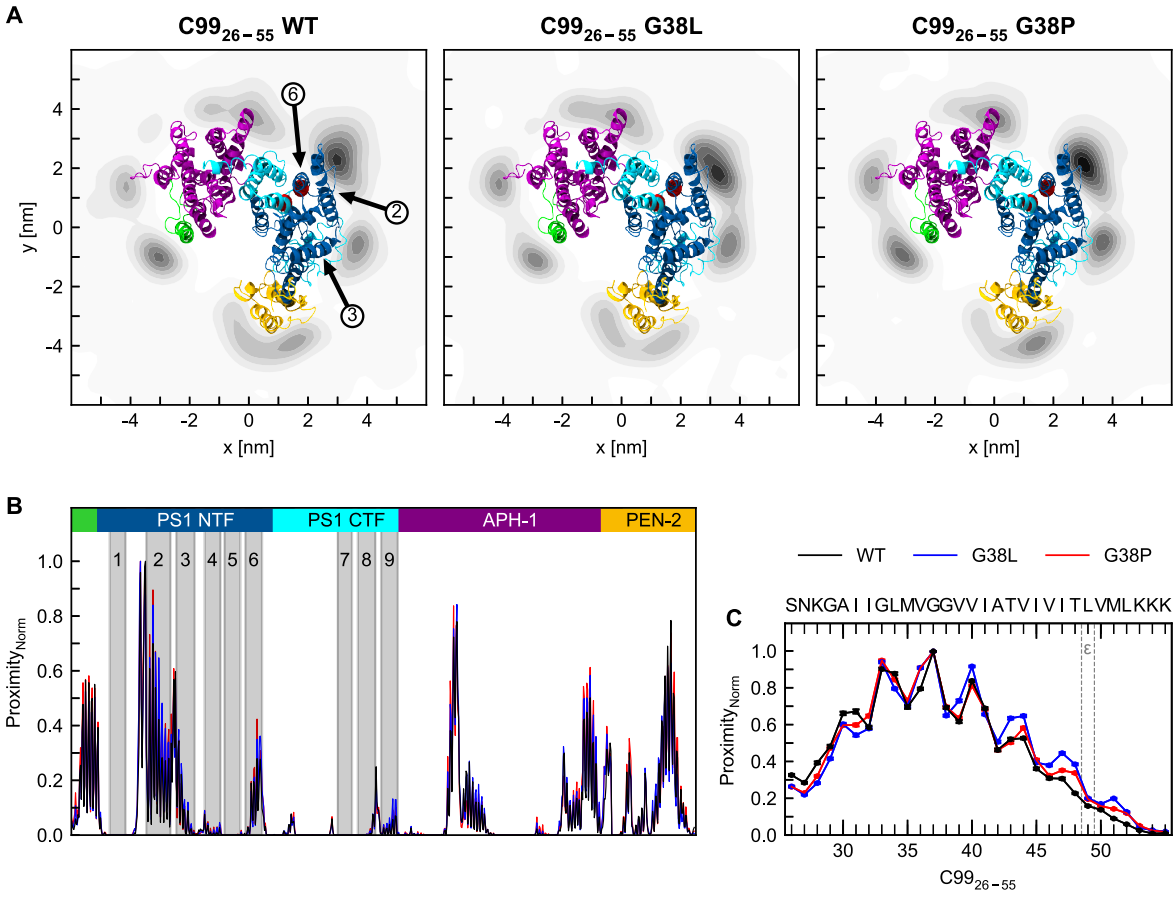

Figure 6. Probability of initial contacts of $C99_{26-55}$ peptides with γ-secretase is not altered for G38 mutants compared to WT in *in silico* modeling of the encounter complex. (**A**) Kernel densities of the center-of-mass location of the $C99_{26-55}$ peptide. Darker colors indicate higher contact probabilities. The representation shows the parts of γ-secretase that are embedded in the membrane, pertaining to the subunits nicastrin (green), APH-1a (purple), PS1 NTF (blue), PS1 CTF (cyan) and PEN-2 (yellow). TMD2, TMD3

and TMD6 of PS1 are highlighted by black arrows, the active site aspartate residues in PS1 TMD6 and TMD7 are indicated by red spheres. (**B**) Normalized proximities between γ-secretase and the $C99_{26-55}$ peptide. Grey areas indicate residues that are part of the indicated TMDs of PS1. (**C**) Normalized proximities between $C99_{26-55}$ and TMD2 of PS1. Contact probabilities are given by the proximity metrics that reports the mean of the closest distance between a set of atoms, where closer distances get a higher weight.

Discussion

Intramembrane proteases are enzymes that in most cases cleave single span membrane protein substrates in their α-helical TMDs, a process which may be generally slow compared to soluble proteases (22). As shown for γ-secretase and rhomboids, recognition of a substrate involves its binding to one or more initial binding site(s) of the protease, so called exosite(s), and subsequent transfer of its TMD to allow access of the enzyme's active site to the scissile bond (21). In the active site instability or even partial unwinding of the substrate α-helix at the cleavage sites is required for proteolysis (36,77). Thus, conformational flexibility of the substrate on a variety of length- and time-scales may play a key role for substrate recruitment and cleavage by γ-secretase. In this study, we focused on the influence of intrinsic structural and dynamical properties of the C99 TMD on its cleavability by γ-secretase. To this end, we asked whether altered cleavability could be correlated with altered conformational dynamics of the C99 TMD and, if so, what kind of dynamics is functionally relevant.

As indicated by previously determined NMR structures in detergent micelles (55,78), as well as by MD simulations in membrane bilayers (38,40,41,79,80), the C99 TMD contains a flexible hinge region at the $G_{37}G_{38}$ residues that allows the helix to adapt to the lipid environment. In particular, the TMD has a straight helical conformation in a bilayer,

but explores kinked α-helical conformation in small detergent micelles (40,55). Since substrate entry of C99 into the active site of γ-secretase may involve swinging-in of the TMD-C containing the cleavage region (43), we hypothesized that the bending flexibility induced by the $G_{37}G_{38}$ hinge could possibly play an important role for the cleavage of this γ-secretase substrate. To investigate this issue, two mutations were investigated that were chosen with the aim to severely alter TMD flexibility by either stabilizing or destabilizing it. The structural and dynamical properties of WT and mutant C99 TMD model peptides were investigated in a POPC bilayer as well as in TFE solution containing 20% water to mimic the interior of the enzyme (50). CD and solution NMR experiments confirmed our rationale that exchanging G38 with leucine leads to a more stable helix, while the G38P mutation reduced helicity. Strongly reduced cleavage efficiency was observed for both mutants in the C99 γ-secretase cleavage assay. This was remarkable since we previously observed that cleavage of C99 was not impaired and rather enhanced when G38 is replaced by the photocrosslinkable, unnatural and bulky amino acid *p*-benzoyl-L-phenylalanine, suggesting that, in principle, this position within the C99 TMD is quite tolerant to structural modifications (21). Interestingly, the processivity of γ-secretase was also altered, particularly for the G38L mutant. Thus, the G38L mutant was almost completely trimmed to Aβ37, whereas the G38P mutant was processed mostly to Aβ40 as for the WT. However, for this mutant the generation of shorter species was shifted exclusively to Aβ39. These observations show that the G38 mutations had a dramatic impact on both the initial cleavability at the ε-site and the subsequent carboxy-terminal trimming by γ-secretase.

A possibility to explain the impaired cleavage of both G38 mutants of the C99 substrate would be an altered substrate encounter. The ssNMR measurements and corresponding MD simulations revealed a moderate tilt angle and no significant differences between the G38 mutants and WT with regard to the predominant tilt and azimuthal angles of the $C99_{26\text{-}55}$ peptide in a bilayer. Additionally MD simulations of the initial contact sites

between the $C99_{26-55}$ peptide and γ-secretase in a POPC bilayer did not disclose major differences between the G38 mutants and WT. Interestingly, consistent with previous studies (21), particularly the PS1 NTF subunit of γ-secretase was found as major contact region. However, substrate contacts in the catalytic cleft of the γ-secretase complex were not found. It is likely that relaxations of the enzyme-substrate complex after binding as well as the substrate transfer to the active site take more time than the ~300 μs total simulation time per peptide used in this analysis.

Subsequently, we assessed whether alterations in the backbone dynamics in the proximity of the residues at the ε-sites, caused by the G38 mutations, would give insight on the altered cleavability of the mutants. DHX and HDX experiments that report on the stability of H-bonds in the C99 TMD revealed differences between WT, G38L, and G38P, in agreement with the observed structural changes. Thus, compared to WT, the overall D/H exchange kinetics was slower for G38L and faster for G38P, as expected. A more detailed residue-specific study revealed that the effect of the G38 mutations on D/H exchange only occurred at the residues in the vicinity of the $G_{37}G_{38}$ hinge while residues in the proximity of the ε-sites were not affected. For these sites, MS-ETD-DHX, NMR-HDX and MD simulations consistently reported low exchange rates. MD simulations further revealed protection of the backbone amides at the ε-sites by stable intrahelical H-bonds. Mutation-induced loosening of the H-bonds or shifting populations of α- and 3_{10} -H-bonds was not observed. These observations show that backbone dynamics at the ε-sites are not affected by the G38 mutations and can thus not explain the reduced cleavage by γ-secretase of both the G38L and G38P mutations of C99. Interestingly, D/H exchange rates at the γ-cleavage sites of the $C99_{26-55}$ peptide were decreased for the G38L mutation and slightly increased for G38P compared to WT. However, these findings cannot be applied to explain the altered processivity of the mutants, since the backbone dynamics of the shortened C99 TMD may change after the AICD has been cleaved off.

In general, α-helical structures of TMDs are stabilized by van der Waals interactions, as well as a strong H-bond network between i and i+3 or i+4 neighbors. Remarkably, for the C99 TMD, water accessibility in the TMD-C has been reported to be extremely limited (38), consistent with our findings of a very high degree of H-bond occupancy and extremely slow D/H exchange in the TMD-C found here in this study as well as previously for other C99 TMD derived segments (41,47). Interestingly, in the TFE/H_2O environment amide exchange is nevertheless extremely slow indicating that the helix around the ε-sites is quite stable. Thus, helix instability is not an intrinsic property of the TMD-C at all, and is also not modulated by our G38 mutations. It appears that opening of the α-helix of the residues in the vicinity of the ε-sites might be the major hurdle for substrate cleavage and is induced only upon an interaction with the enzyme. Although these results confirm previous studies (41,42,47), they are in contrast with a recent study by Cao et al (81), who calculated D/H fractionation factors from ratios of exchange rates in order to determine H-bond strengths of C99 in lysomyristoyl-phosphatidyl glycerol micelles. In this environment the C99 TMD was found to be artificially kinked (55). Most residues were classified as having strong H-bonds (up to 6 kcal/mol) but some residues in TMD-N and particularly in TMD-C (T43, V44 and T48) were interpreted as having highly labile H-bonds. However, as explained elsewhere (60), H-bond strengths derived by the approach of Cao et al (81) describe the preference for deuterium in an amide-to-solvent H-bond rather than the properties of the intrahelical amide-to-carbonyl H-bonds.

Models of enzymatic substrate processing provide evidence that conformational dynamics of substrates and enzymes play a key role for recognition and relaxation steps. Here, the intrinsic dynamics already encompass all the conformations necessary for substrate binding, pre-organization of the substrate-enzyme complex and stabilization of the transition state (82-85). The chemical reaction is thought to be a rare, yet rapid, event (86), that occurs only after sufficient conformational sampling of the enzyme-substrate complex

to generate a configuration that is conducive to the chemical reaction. This sampling could be at the level of substrate transfer from exosites to the active site as well as at the level of substrate fitting into the active site and series of relaxations and mutual adaptation steps of substrate and enzyme after initial binding might be required before the scissile bond fits into the active site of γ-secretase. Thus, multiple conformational selection steps may play a decisive role to distinguish between substrates and non-substrates (84).

Large-scale shape fluctuations might be selected to enable recognition, while lower-amplitude, more localized motions help to optimize and stabilize the enzyme-bound intermediate states (82-85,87). The essential property enabling the TMD to switch between different shapes of functional importance is the organization of rigidity/flexibility along the helix backbone where residues enjoying higher flexibility can coordinate the motions of more rigid flanking segments. These flexible hinges might provide the necessary bending and twisting flexibility for orienting the reaction partners properly. With regard to C99, our MD analyses here and previously (48) revealed that the residues $T_{43}VI_{45}$ upstream to the ε-sites provide hinge flexibility as well. In addition to bending around the $G_{37}G_{38}$ sites, twisting and more complex collective motions including combinations of bending and twisting around the pair of hinges can occur. This structural distribution translates into a diversity of ε-site orientations. The perturbation of this distribution might provide plausible explanations of the reduced cleavability of both, the G38L and the G38P mutant. Particularly, the counter-clockwise shifts of the orientation of the ε-sites for both G38L and G38P mutants in POPC and the absence of small bending angles for G38P indicate that presentation of the scissile bond to the active site of presenilin can be misdirected for each mutant in its own way and differently compared to WT. The modified mechanical linkage of helical segments constituting the substrate TMD might increase the probability of non-productive interactions with the enzyme what could explain the reduced cleavability of the

G38 mutants. A similar mechanism was proposed recently to explain reduced ε-cleavage efficiency induced by FAD mutations upstream to the ε-sites in the C99 TMD (48,88).

Notably, the TMD of Notch1, as well as the TMD of the integrin receptor (IR), two other substrates of γ-secretase (9), have conformations very different from that of the C99 TMD as determined from solution-NMR of single-span TM helices in membrane mimics (89,90). In particular, Notch1 appears to be a straight helix, while the TMD helix of the integrin receptor is S-shaped resembling the minor population of double-hinge conformations of the C99 TMD in a POPC bilayer found in our study. These observations seem to challenge the swinging-in model coordinated by a central hinge as an integral step for the passage of the substrate toward the active site. Nevertheless, generally the conformational repertoire of the TMD of the substrates is determined by α-helical folding where helices bend and twist around several sites. The relative importance of the individual conformations reflects differences in local flexibility. Functionally relevant conformations are not necessarily among the highest populated ones. Rather conformations for which the protein has a low intrinsic propensity might be selected for productive interactions with the enzyme regulating or coordinating mechanistic stages preceding catalysis. These so-called 'hidden', 'invisible' or 'dark' states are amenable by NMR or MD methods (87,91-93). For the C99 TMD we recently demonstrated by *in silico* modeling the functional importance of a flexible hinge localized in TMD-C at $T_{43}VI_{45}$ for conformational adaptation of the TMD to interactions with the enzyme where large-scale bending is obstructed (48). Although missing large-scale helix bending, Notch1 and IR (and even other substrates of γ-secretase) might nevertheless provide the repertoire of functionally important motions necessary to adapt to interactions with the enzyme at different stages of the catalytic cycle. Furthermore, binding and conformational relaxation steps of different substrates might follow different pathways to optimize the catalytic competent state (83,84).

Taken together, we conclude that necessary conformational relaxations required to facilitate the proteolytic event at the active site are not due to intrinsically enhanced flexibility of the C99 substrate around its cleavage site, but are induced by interactions of the substrate with the enzyme. Interestingly, in line with the interpretation of our data, it has recently been shown by vibrational spectroscopy that PSH, an archaeal homolog of presenilin, can induce an extended β-strand geometry in the center of the TMD of Gurken, a native substrate of the bacterial rhomboid GlpG, while GlpG induces local transitions to a more open 3_{10} conformation at its N-terminal end (77). Conformational flexibility of substrate and enzyme is necessary to prepare access to the cleavage site and orient the reaction partners properly. Conformational adaptability of the C99 substrate TMD is provided by flexible regions coordinating motions of helical segments. Subtle changes of H-bond flexibility induced around the $G_{37}G_{38}$ hinge by G38 mutations change mechanical linkage there and misdirect the orientation of the initial cleavage sites thus diminishing the probability of productive orientation with the active site of γ-secretase and impairing cleavage irrespective of whether the mutation is helix stabilizing of helix destabilizing.

Materials and Methods

Materials

1-Palmitoyl-2-oleoyl-*sn*-glycero-3-phosphocholine (POPC) as well as *sn*-1 chain perdeuterated POPC-d_{31} were purchased from Avanti Polar Lipids. 1,1,1-3,3,3-Hexaflouroisopropanol (HFIP) and 2,2,2-trifluoroethanol (TFE) were purchased from Sigma Aldrich.

Peptides

For all circular dichroism (CD), solution NMR, ssNMR and DHX experiments $C99_{26\text{-}55}$, a 30 amino acid long peptide comprising residues 26 to 55 of C99 (C99 numbering, see **Figure 1A**), with N-terminal acetylation and C-terminal amidation was used. WT peptide and G38L and G38P mutants thereof (**Table 1**) were purchased from Peptide Specialty Laboratories GmbH, Heidelberg, Germany and from the Core Unit Peptid-Technologien, University of Leipzig, Germany. For ssNMR, A30, G33, L34, M35, V36, G37, A42, and V46 were labeled in the WT sequence with ^{13}C and ^{15}N. In the two mutant peptides, only A30, L34, G37, and V46 were labeled. For ETD measurements, peptides with a modified N-terminal anchor (**Table 1**) were used. In all cases purified peptides were to >90 % purity as judged by mass spectrometry.

Table 1: Sequences of investigated peptides

Name	Sequence
$C99_{26\text{-}55}$	Ac-SNKGAIIGLMVG**G**VVIATVIVITLVMLKKK-NH_2
$C99_{26\text{-}55}$ G38L	Ac-SNKGAIIGLMVG**L**VVIATVIVITLVMLKKK-NH_2
$C99_{26\text{-}55}$ G38P	Ac-SNKGAIIGLMVG**P**VVIATVIVITLVMLKKK-NH_2
KKK-$C99_{26\text{-}55}$	Ac-KKKGAIIGLMVGGVVIATVIVITLVMLKKK-NH_2

γ-Secretase *in vitro* assay

C99-based WT and mutant substrates were expressed in *E. coli* as C100-His_6 constructs (C99 fusion proteins containing an N-terminal methionine and a C-terminal His_6-tag) (52) and purified by Ni-NTA affinity-chromatography. To analyze their cleavability by γ-secretase, 0.5 μM of the purified substrates were incubated overnight at 37 °C with detergent-solubilized HEK293 membrane fractions containing γ-secretase as described (53). To control for specific cleavage by γ-secretase, substrates were incubated at 37 °C with 0.5 μM of the γ-secretase inhibitor L-685,458 (Merck Millipore) or incubated at 4 °C as a control. Generated Aβ was analyzed with immunoblotting using antibody 2D8 (94) and quantified by measuring the chemiluminescence signal intensities with the Fluorochem™ 8900 detection system (Alpha Innotech). Analysis of γ-secretase activity was repeated with three independent substrate purifications in three technical replicates for each of the constructs.

Mass spectrometry analysis of Aβ species

Aβ species generated in the γ-secretase vitro assays were immunopreciptated with 4G8 antibody (Covance) and subjected to mass spectrometry analysis on a 4800 MALDI-TOF/TOF Analyzer (Applied Biosystems/MDS SCIEX) as described previously (95,96).

CD spectroscopy

$C99_{26-55}$ WT, G38L and G38P mutant peptides were incorporated into large unilamellar vesicles (LUV) composed of POPC at a lipid/protein molar ratio of 30:1. First, 500 μg peptide and 3.72 mg POPC were co-mixed in 1 ml HFIP. After evaporation of the HFIP, the mixture was dissolved in 1 ml cyclohexane and lyophilized. The resulting fluffy powder

was dissolved in 977 µl buffer (10 mM sodium phosphate, pH 7.4). After 10 freeze-thaw cycles, LUVs were prepared through extrusion using a 100-nm polycarbonate membrane and a LipofastTM extruder device (Armatis GmbH, Weinheim, Germany). CD spectra were recorded with a Jasco 810 spectropolarimeter. A cuvette with a 1 mm path length was filled with 200 µl of the LUV/$C99_{26-55}$ preparation in which the final peptide concentration was 83 µM and the lipid concentration 2.5 mM. The UV absorbance 210 nm of the WT peptide was used as a reference to normalize the final concentration of the reconstituted mutant peptides. Alternatively, the peptides (50 µM final concentration) were dissolved in TFE/H_2O (80/20 v/v) and concentrations were determined based on the using the UV absorbance of the peptide bond at 205 nm with an extinction coefficient ε_{205} = 73.600 $M^{-1}cm^{-1}$. The latter was determined by calibration with a homologous peptide SNK**W**GAIIGLMVGGVVIATVIVITLVMLKKK whose concentration was determined using the ε_{280} = 5600 $mol^{-1}cm^{-1}$ of the additional tryptophan. Mean molar residue ellipticities ([Θ]) were calculated based on the peptide concentrations.

Solution NMR

Dry $C99_{26-55}$ WT ($^{15}N/^{13}C$ -labeled at positions G29, G33, G37, G38, I41, V44, M51 and L52), G38L and G38P mutant peptides were dissolved in 500 µL 80 % trifluoroethanol-d3 (TFE-d3) and 20 % H_2O respectively. pH was adjusted to 5.0 by adding the corresponding amount of NaOH. Peptide concentrations ranged between 50 to 500 µM. The NMR spectra of the peptides were obtained on a 600 MHz AVANCE III spectrometer (Bruker BioSpin, Rheinstetten, Germany) equipped with a TXI cryoprobe at a temperature of 300 K. To assign ^{1}H and ^{13}C-resonances of the peptides a set of two-dimensional spectra was recorded: ^{1}H-^{1}H-TOCSY with a mixing time of 60 ms, ^{1}H-^{1}H-NOESY with a mixing time of 200 ms, and ^{1}H-^{13}C-HSQC. Spectra were recorded with 24 scans and 1000 data points in the indirect dimension. The NMR spectra were analyzed using NMRViewJ (One Moon Scientific).

For hydrogen-deuterium (H/D) NMR-HDX exchange measurements dry peptides were dissolved in 80 % TFE-d3 and 20 % D_2O. Measurements were done at at least three different pH-values to access all exchangeable protons, using the correlation of exchange rate and pH value. pH was adjusted using NaOD and DCl. Eleven TOCSY or ClipCOSY (97) spectra with an experimental time of 3 h 26 min each (mixing time 30 ms, 24 scans, 300 data points in the indirect dimension) were acquired sequentially. Additionally eleven ^{1}H-^{15}N-HSQC spectra of the WT were recorded (2 scans, 128 points in the indirect dimension) in between.

Exchange of the first five to six and the last two residues was too fast to measure. M35 and A42 cross peak intensities were significantly lower than those of other amino acids. The H/D exchange rate constant ($k_{exp,HDX}$) were obtained fitting the cross peak intensities over time to equation 1:

$$y = c + a \cdot e^{(-k_{exp,DHX} \cdot t)} \quad (1)$$

where t is time, a and c are constants. Rate constants were calculated for all three pH values and then scaled to pH 5.

Solid-state NMR

Multilamellar vesicles were prepared by co-solubilizing POPC and the used $C99_{26-55}$ peptide in HFIP at a 30:1 molar ratio. After evaporation of the solvent in a rotary evaporator, the sample film was dissolved by vortexing in cyclohexane. Subsequently, the samples were lyophilized to obtain a fluffy powder. The powder was hydrated with buffer (100 mM NaCl, 10 mM Hepes, pH 7.4) to achieve a hydration level of 50% (w/w) and homogenized by 10 freeze-thaw cycles combined with gentle centrifugation.

^{13}C magic-angle-spinning (MAS) NMR experiments were performed on a Bruker Avance III 600 MHz spectrometer (resonance frequency 600.1 MHz for ^{1}H, 150.9 MHz for ^{13}C) using 4 mm and 3.2 mm double-resonance MAS probes. The cross-polarization contact time was 700 µs, typical lengths of the 90° pulses were 4 µs for ^{1}H, 5 µs for ^{15}N and 4-5 µs for ^{13}C. For heteronuclear two pulse phase modulation (TPPM) decoupling, a ^{1}H radio-frequency field of 62.5 kHz was applied. ^{13}C chemical shifts were referenced externally relative to tetramethylsilane. ^{1}H-^{13}C and ^{1}H-^{15}N dipolar couplings were measured by constant-time DIPSHIFT experiments using frequency-switched Lee Goldburg for homonuclear decoupling (80 kHz decoupling field) (98). The ^{1}H-^{13}C dipolar coupling was determined by simulating dipolar dephasing curves over one rotor period. These dipolar couplings were divided by the known rigid limit as reported previously (99). MAS experiments for the site-dependent order parameter were carried out at a MAS frequency of 3 kHz and a temperature of 30°C.

DIPSHIFT ^{1}H-^{13}C order parameters were analyzed with a variant of the established GALA model (66). While in the GALA model ^{2}H NMR order parameters of C_β-$^{2}H_\beta$ bonds of alanin residues are used, we utilized DIPSHIFT order parameters of the $^{13}C_\alpha$-$^{1}H_\alpha$ bond vectors. These order parameters were analyzed with a model in which the $C99_{26\text{-}55}$ peptide is described as a perfect TMD helix (with α-helix pitch of 100° between neighboring amino acids). Internal motions of the helix that average the dipolar interaction tensor were described by an internal order parameter as used in some variants of the GALA model (63,100,101). To reduce the number of fitting parameters, the internal order parameter was determined from MD simulations by alignment of all peptide structures and subsequent C_α-H_α bond order parameter calculation. The obtained value of 0.95 was used as a fixed scaling factor of the dipolar interaction along the $^{13}C_\alpha$-$^{1}H_\alpha$ bond in our model.

The orientation of the helix in the membrane is described by means of the tilt angle τ and the azimuthal rotation angle ρ (amino acid S26 was used as the reference for ρ) and the

orientation of the $^{13}C_\alpha$-$^{1}H_\alpha$ bond in the helix was described by the internal angle β. These three angles represent the variable parameters of our model which were varied in 1° steps in the intervals 0°-90° (τ), 0°-359° (ρ), and 54°-74° (β). For each possible combination of these three parameters the $^{13}C_\alpha$-$^{1}H_\alpha$ order parameter was calculated (details of the calculation below) and compared to the measured values via calculation of the RMSD. For better visualization the 3D matrix of RMSD values (where each dimension corresponds to one variable parameter) was then reduced to a 2D representation where the internal angle β is omitted. This was achieved by taking each (τ, ρ) pair and projecting the minimal RMSD of all possible β values onto the (τ, ρ) plane.

The needed internal angles α = -50.2° and β = 64.0° (which was then varied in a ±10° range) for C_α-H_α bonds were determined from model helices with ideal backbone torsion angles of φ = -57° and ψ = -47° built with the molefacture plugin of VMD (63,102). All angles were defined as described in (63). The tilt angle τ was varied between 0° and 90°, the azimuthal angle ρ between 0° and 359° (amino acid S26 was used as the reference for ρ) and the internal angle β between 54° and 74°. All three angles were varied in 1° steps and the resulting C_α-H_α bond orientations of the labeled amino acids were used to calculate their dipolar interaction tensor in the laboratory frame. Since the C_α-H_α order parameters were not measured on macroscopically aligned samples as in the ^{2}H NMR measurements used for the GALA model, the rotation of the peptide as a whole about the membrane normal needed to be averaged out on the timescale of NMR experiment (~40 μs). This was checked in the MD simulations and it could be shown that the rotation is almost completely averaged out even on the MD simulation timescale of 2.5 μs. Also, ^{2}H (100-102) and ^{31}P NMR spectra (103) of oriented samples at 90° orientation show that this rotation is averaged out for transmembrane peptides of the WALP family on the timescale of the ^{2}H (~6 μs) and ^{31}P (~20 μs) NMR experiments. Therefore, the previously calculated dipolar interaction tensor in the laboratory frame was averaged about the membrane normal and the resulting average

tensor used to predict the C_α-H_α DIPSHIFT order parameter for the particular (τ,ρ,β) combination using a previously published procedure (104). Finally, the error weighted RMSD to the experimental order parameters was determined for all possible (τ,ρ,β) combinations and stored in a 3D representation. For better visualization this matrix of RMSD values was then reduced to a 2D representation where the internal angle β is omitted. This was achieved by taking each (τ, ρ) pair and projecting the minimal RMSD of all possible β values onto the (τ, ρ) plane.

Mass spectrometric experiments of Deuterium/Hydrogen exchange (MS-DHX)

All mass spectrometric experiments were performed on a Synapt G2 HDMS (Waters Co., Milford, MA). A 100 µl Hamilton gas-tight syringe was used with a Harvard Apparatus 11plus, the flow rate was set to 5 µl/min. Spectra were acquired in a positive-ion mode with one scan for each second and 0.1 s interscan time.

Solutions of deuterated peptide (100 µM in 80 % (v/v) d1-trifluoroethanol (d1-TFE) in 2 mM ND_4-acetate) were diluted 1:20 with protiated solvent (80 % (v/v) TFE in 2 mM NH_4-acetate, pH 5.0) to a final peptide concentration of 5 µM and incubated at a temperature of 20.0°C in a thermal cycler (Eppendorf, Germany). At the used peptide concentration of 5 µM, the peptides remain monomeric (41). Incubation times were 0, 1, 2, 5, 10, 20, 30, 40, 50 min, and 1, 2, 3, 4, 6, 8, 12, 24, 48, 72 h. Exchange reactions were quenched by placing the samples on ice and adding 0.5 % (v/v) formic acid, resulting in a pH ≈ 2.5. Mass/charge ratios were recorded and evaluated as previously described, (56,57) including a correction for the dilution factor. For electron transfer dissociation (ETD) we preselected the 5+ charged peptides via MS/MS and used 1,4- dicyanobenzene as reagent. Fragmentation of peptides was performed as described. (57). Briefly, ETD MS/MS scans were accumulated over 10 min scan time, smoothed (Savitzky-Golay, 2 x 4 channels), and centered (80% centroid top, heights, 3 channels). MS-ETD-measurements were performed

after 13 different incubation periods (from 1 min to 3 d) where exchange took place at pH 5.0. Shorter (0.1 min, 0.5 min) and longer (5 d, 7 d) incubation periods were simulated by lowering the pH to 4.0 or elevating pH to 6.45, respectively, using matched periods. The differences to pH 5.0 were considered when calculating the corresponding rate constants. We note that base-catalyzed exchange is responsible for at least 95 % of total deuteron exchange at pH 4.0 and above. The resulting ETD c and z fragment spectra were evaluated using a semi-automated procedure (MassMap_2017-11-16_LDK Software, MassMap GmbH & Co. KG, Wolfratshausen) (37). The extent of hydrogen scrambling could not be calculated with the ammonia loss method due to the blocked N-termini. However, previous experiments with similar peptides showed scrambling to be negligible under our conditions. (32). During all MS-DHX experiments, a gradual shift of monomodal shaped isotopic envelopes towards lower mass/charge values was observed. This is characteristic for EX2 kinetics with uncorrelated exchange of individual deuterons upon local unfolding (58,105).

Molecular Dynamics (MD) simulations

The sequences of the investigated model peptides are shown in **Table 1**. Because no conformations were available for the G38 mutants, we used a stochastic sampling protocol to generate a set of 78 initial start conformations (for details see (60)).

For all-atom simulations in a rectangular solvent box, containing 80 % TFE and 20 %TIP3 (v/v) each start conformation was simulated for 200 ns using (settings as described in (41)). Production runs were performed in a NPT ensemble (T = 293 K, p = 0.1 MPa) using NAMD 2.11 (106) and the CHARMM36 force field (107). The last 150 ns of each simulation were subjected to analysis, leading to an effective aggregated analysis time of 11.7 µs for each peptide. Frames were recorded every 10 ps.

For all-atom simulations in POPC bilayers, the 78 conformations were hierarchically clustered, the centroid of the cluster with the highest population was placed in a symmetric

bilayer, consisting of 128 POPC lipids, using protocols as provided by CHARMM-GUI (108). Simulations of 2.5 µs (T = 303.15 K, p = 0.1 MPa) were performed, using NAMD 2.12 (106), the CHARMM36 force field (107) and settings as provided by CHARMM-GUI. Frames were recorded every 10 ps. Only the last 1.5 µs of the trajectory were subjected to analysis.

Occupancies of closed H-bonds were computed for α- and 3_{10}-H-bonds. Thereby, a H-bond was considered to be closed if the $O \cdots H$ distance was < 0.26 nm and the $O \cdots H - N$ angle was in the range 180° ± 60°. H-bonds of each helix type for any amide i are considered to be closed if either the H-bond to O_{i-4} (α H-Bond) or the H-bond to O_{i-3} (3_{10} H-bond) is formed.

The tilt angle (τ) was computed as the inner product between the membrane normal vector (z-axis) and the TM-helix axis vector. The helical axis vector is computed by singular value decomposition of the helix axis points determined from a differential geometric approach (88). Azimuthal rotation angles ρ were computed as described in (63). The C_α atom of G33 was used as reference instead of the first residue of the helix.

Hinge bending and twisting motions in the TMD helix were analyzed with the Dyndom program (72) as described in (32,48), where snapshots taken every 100 ps were subjected to analysis. All visuals were generated by VMD 1.9.2 (109).

DHX kinetics were calculated from the MD simulations as described in (32). In order to account for non-deuterated residues in the experiment, the exponential function was modified as shown in equation 2:

$$D(t) = \sum_{i=1}^{n_{res}} \left(A * e^{-k_i * f * (t+t_0)} + c \right) \quad (2)$$

To account for the 5% of non-deuterated peptides in the experiment, the amplitude (A) is set to 0.95 and a baseline (c) of 0.05 is added. In addition to the original protocol, we added a

second fitting parameter t_0, which accounts for time delays in experiment. The quality of the MD-derived prediction of exchange kinetics was assessed by the normalized mean-squared deviation (χ^2) of the average D(t) values with respect to the experimental averages.

For statistical evaluation of MD results, mean values and 95% confidence intervals were obtained by bias-corrected and accelerated bootstrap resampling (110) of block averages. Block averages were computed from blocks of 30 ns and 10000 bootstrap samples were generated from the block averages. Thereby, values for each residue in a block were considered as dependent. The block size was chosen to be $> 2\tau$, with τ representing the autocorrelation function's first zero-passage time. Distributions of τ values for each parameter are shown in **Figure S7**. Error propagation was performed by Monte-Carlo sampling using 10000 Monte-Carlo samples. As for bootstrap resampling, values for each residue in a block were considered to be dependent.

Coarse-grained MD simulations in POPC were performed according to the slightly modified DAFT approach as described in Wassenaar et al. (73). For each setup 1000 pairs consisting of a single C99 TMD and γ-secretase were randomly rotated and inserted in a fully hydrated membrane bilayer, containing 500 POPC lipids. Structures of the C99 TMD were taken from the all-atom simulations in POPC and transformed to a coarse-grained representation (111). To mimic the low amplitude dynamics of γ-secretase, we used the GoMARTINI model (75) which adds a network of Lennard−Jones like bonds between the Martini backbone beads, in order to provide a dynamic behavior close to an all-atom representation. The strength of these bonds was adjusted to 1.5 times the strength of a hydrogen bond in order to reproduce site-specific RMSF profiles of a 1 μs all-atom simulation of γ-secretase in POPC. The network was created based on a contact-map built from the overlap of van der Waals radii and the chemical nature of the residues (75,112). The all-atom results were kindly provided by Martin Zacharias (TUM) and contained the membrane part of γ-secretase, without the extracellular part of nicastrin. Equilibration and

production runs were performed according to the DAFT protocol using GROMACS 5.1(113) with the Martini 2.2 force field (114). Thereby, 1 µs of free dynamics were sampled for each replicate, using a NPT ensemble (T = 303 K, p = 1013 hPa). The last 500 ns of each successfully run simulation were analyzed.

To analyze the substrate-enzyme contact**,** proximities were calculated for every backbone Martini bead of γ-secretase and the $C99_{26\text{-}55}$ TMD. Distances d_{ij} (in nm) were computed every 100 ns and transformed to proximities according to equation 3 with $d_0 = 0.93$ nm.

$$p_{ij} = e^{-\left(\frac{d_{ij}}{d_0}\right)^6} \qquad (3)$$

The proximities of each pair were averaged over all analyzed frames and replicates. In order to compute a residue's normalized proximity to a group of other residues, all proximities between that residues and the group are summed up. Proximities for a sequence of residues were normalized by the highest proximity within that sequence.

Acknowledgements

This work was supported by the DFG (FOR2290) (D.H., B.L., D.L., C.S., H.S.) and in part by the VERUM foundation (F.K.). Computing resources were provided by the Leibniz Computing Center through grant p292so as well as by the Gauss Centre for Super Computing through grant pr48ko. We thank Martin Zacharias for providing results of all-atom simulations of γ-secretase and Marius Lemberg for critical reading of the manuscript

Author contributions

D.H., B.L., D.L., C.S., C.M.-G., H.S. conceived the study, designed experiments, analyzed and interpreted data, and supervised research. A.G. and S.M. performed MD simulations, F.K. CD spectroscopy, N.M. cleavage assays, P.H. hydrogen/deuterium exchange experiments, and M.S., H.H., A.V., H.F. NMR spectroscopy. A.G., S.M., F.K., N.M., P.H., M.S., H.H., A.V., H.F. analyzed and interpreted data. F.K. coordinated the drafting of the manuscript. F.K., C.M.-G., A.G., C.S. and H.S. wrote the manuscript with contributions of all authors.

References:

1. Wolfe, M. S. (2009) Intramembrane-cleaving proteases. *J Biol Chem* **284**, 13969-13973
2. Sun, L., Li, X., and Shi, Y. (2016) Structural biology of intramembrane proteases: mechanistic insights from rhomboid and S2P to γ-secretase. *Curr Opin Struct Biol* **37**, 97-107
3. Lemberg, M. K., and Martoglio, B. (2002) Requirements for signal peptide peptidase-catalyzed intramembrane proteolysis. *Mol Cell* **10**, 735-744
4. Fluhrer, R., Martin, L., Klier, B., et al. (2012) The α-helical content of the transmembrane domain of the British dementia protein-2 (Bri2) determines its processing by signal peptide peptidase-like 2b (SPPL2b). *J Biol Chem* **287**, 5156-5163
5. Ye, J., Dave, U. P., Grishin, N. V., et al. (2000) Asparagine-proline sequence within membrane-spanning segment of SREBP triggers intramembrane cleavage by site-2 protease. *Proc Natl Acad Sci U S A* **97**, 5123-5128
6. Linser, R., Salvi, N., Briones, R., et al. (2015) The membrane anchor of the transcriptional activator SREBP is characterized by intrinsic conformational flexibility. *Proc Natl Acad Sci U S A* **112**, 12390-12395
7. Steiner, H., Fluhrer, R., and Haass, C. (2008) Intramembrane proteolysis by γ-secretase. *J Biol Chem* **283**, 29627-29631
8. De Strooper, B., Iwatsubo, T., and Wolfe, M. S. (2012) Presenilins and γ-secretase: structure, function, and role in Alzheimer Disease. *Cold Spring Harb Perspect Med* **2**, a006304

9. Haapasalo, A., and Kovacs, D. M. (2011) The many substrates of presenilin/γ-secretase. *J Alzheimers Dis* **25**, 3-28

10. Jurisch-Yaksi, N., Sannerud, R., and Annaert, W. (2013) A fast growing spectrum of biological functions of γ-secretase in development and disease. *Biochim Biophys Acta* **1828**, 2815-2827

11. Holtzman, D. M., Morris, J. C., and Goate, A. M. (2011) Alzheimer's disease: the challenge of the second century. *Sci Transl Med* **3**, 77sr71

12. Selkoe, D. J., and Hardy, J. (2016) The amyloid hypothesis of Alzheimer's disease at 25 years. *EMBO Mol Med* **8**, 595-608

13. Lichtenthaler, S. F., Haass, C., and Steiner, H. (2011) Regulated intramembrane proteolysis--lessons from amyloid precursor protein processing. *J Neurochem* **117**, 779-796

14. Takami, M., and Funamoto, S. (2012) γ-Secretase-dependent proteolysis of transmembrane domain of amyloid precursor protein: successive tri- and tetrapeptide release in amyloid β-Protein production. *Int J Alzheimers Dis* **2012**, 591392

15. Bolduc, D. M., Montagna, D. R., Seghers, M. C., et al. (2016) The amyloid-β forming tripeptide cleavage mechanism of γ-secretase. *Elife* **5**

16. Weggen, S., and Beher, D. (2012) Molecular consequences of amyloid precursor protein and presenilin mutations causing autosomal-dominant Alzheimer's disease. *Alzheimers Res Ther* **4**, 9

17. Cacace, R., Sleegers, K., and Van Broeckhoven, C. (2016) Molecular genetics of early-onset Alzheimer's disease revisited. *Alzheimers Dement* **12**, 733-748

18. Hemming, M. L., Elias, J. E., Gygi, S. P., et al. (2008) Proteomic profiling of γ-secretase substrates and mapping of substrate requirements. *PLoS Biol* **6**, e257

19. Bolduc, D. M., Montagna, D. R., Gu, Y., et al. (2016) Nicastrin functions to sterically hinder γ-secretase-substrate interactions driven by substrate transmembrane domain. *Proc Natl Acad Sci U S A* **113**, E509-518

20. Struhl, G., and Adachi, A. (2000) Requirements for presenilin-dependent cleavage of Notch and other transmembrane proteins. *Mol Cell* **6**, 625-636

21. Fukumori, A., and Steiner, H. (2016) Substrate recruitment of γ-secretase and mechanism of clinical presenilin mutations revealed by photoaffinity mapping. *EMBO J* **35**, 1628-1643

22. Kamp, F., Winkler, E., Trambauer, J., et al. (2015) Intramembrane proteolysis of β-amyloid precursor protein by γ-secretase is an unusually slow process. *Biophys J* **108**, 1229-1237

23. Langosch, D., and Steiner, H. (2017) Substrate processing in intramembrane proteolysis by γ-secretase - the role of protein dynamics. *Biol Chem* **398**, 441-453

24. Madala, P. K., Tyndall, J. D., Nall, T., et al. (2010) Update 1 of: Proteases universally recognize β strands in their active sites. *Chem Rev* **110**, PR1-31

25. Timmer, J. C., Zhu, W., Pop, C., et al. (2009) Structural and kinetic determinants of protease substrates. *Nat Struct Mol Biol* **16**, 1101-1108

26. Belushkin, A. A., Vinogradov, D. V., Gelfand, M. S., et al. (2014) Sequence-derived structural features driving proteolytic processing. *Proteomics* **14**, 42-50

27. Robertson, A. L., Headey, S. J., Ng, N. M., et al. (2016) Protein unfolding is essential for cleavage within the α-helix of a model protein substrate by the serine protease, thrombin. *Biochimie* **122**, 227-234

28. Sato, T., Tang, T. C., Reubins, G., et al. (2009) A helix-to-coil transition at the ϵ-cut site in the transmembrane dimer of the amyloid precursor protein is required for proteolysis. *Proc Natl Acad Sci U S A* **106**, 1421-1426

29. Hu, Y., Kienlen-Campard, P., Tang, T. C., et al. (2017) β-Sheet structure within the extracellular domain of C99 regulates amyloidogenic processing. *Sci Rep* **7**, 17159

30. Ousson, S., Saric, A., Baguet, A., et al. (2013) Substrate determinants in the C99 juxtamembrane domains differentially affect γ-secretase cleavage specificity and modulator pharmacology. *J Neurochem* **125**, 610-619

31. Cao, Z., and Bowie, J. U. (2012) Shifting hydrogen bonds may produce flexible transmembrane helices. *Proc Natl Acad Sci U S A* **109**, 8121-8126

32. Högel, P., Götz, A., Kuhne, F., et al. (2018) Glycine perturbs local and global conformational flexibility of a transmembrane helix. *Biochemistry* **57**, 1326-1337

33. Higashide, H., Ishihara, S., Nobuhara, M., et al. (2017) Alanine substitutions in the GXXXG motif alter C99 cleavage by γ-secretase but not its dimerization. *J Neurochem* **140**, 955-962

34. Oestereich, F., Bittner, H. J., Weise, C., et al. (2015) Impact of amyloid precursor protein hydrophilic transmembrane residues on amyloid-β generation. *Biochemistry* **54**, 2777-2784

35. Olsson, F., Schmidt, S., Althoff, V., et al. (2014) Characterization of intermediate steps in amyloid β (Aβ) production under near-native conditions. *J Biol Chem* **289**, 1540-1550

36. Fernandez, M. A., Biette, K. M., Dolios, G., et al. (2016) Transmembrane substrate determinants for γ-secretase processing of APP CTFβ. *Biochemistry* **55**, 5675-5688

37. Stelzer, W., Scharnagl, C., Leurs, U., et al. (2016) The impact of the 'Austrian' mutation of the amyloid precursor protein transmembrane helix is communicated to the hinge region. *ChemistrySelect* **1**, 4408-4412

38. Dominguez, L., Meredith, S. C., Straub, J. E., et al. (2014) Transmembrane fragment structures of amyloid precursor protein depend on membrane surface curvature. *J Am Chem Soc* **136**, 854-857

39. Langosch, D., Scharnagl, C., Steiner, H., et al. (2015) Understanding intramembrane proteolysis: from protein dynamics to reaction kinetics. *Trends Biochem Sci* **40**, 318-327

40. Lemmin, T., Dimitrov, M., Fraering, P. C., et al. (2014) Perturbations of the straight transmembrane α-helical structure of the amyloid precursor protein affect its processing by γ-secretase. *J Biol Chem* **289**, 6763-6774

41. Pester, O., Barrett, P. J., Hornburg, D., et al. (2013) The backbone dynamics of the amyloid precursor protein transmembrane helix provides a rationale for the sequential cleavage mechanism of γ-secretase. *J Am Chem Soc* **135**, 1317-1329

42. Scharnagl, C., Pester, O., Hornburg, P., et al. (2014) Side-chain to main-chain hydrogen bonding controls the intrinsic backbone dynamics of the amyloid precursor protein transmembrane helix. *Biophys J* **106**, 1318-1326

43. Tian, G., Sobotka-Briner, C. D., Zysk, J., et al. (2002) Linear non-competitive inhibition of solubilized human γ-secretase by pepstatin A methylester, L685458, sulfonamides, and benzodiazepines. *J Biol Chem* **277**, 31499-31505

44. Quint, S., Widmaier, S., Minde, D., et al. (2010) Residue-specific side-chain packing determines the backbone dynamics of transmembrane model helices. *Biophys J* **99**, 2541-2549

45. Altmann, K. H., Wojcik, J., Vasquez, M., et al. (1990) Helix-coil stability constants for the naturally occurring amino acids in water. XXIII. Proline parameters from random poly (hydroxybutylglutamine-co-L-proline). *Biopolymers* **30**, 107-120

46. Sato, C., Morohashi, Y., Tomita, T., et al. (2006) Structure of the catalytic pore of γ-secretase probed by the accessibility of substituted cysteines. *J Neurosci* **26**, 12081-12088

47. Pester, O., Götz, A., Multhaup, G., et al. (2013) The cleavage domain of the amyloid precursor protein transmembrane helix does not exhibit above-average backbone dynamics. *ChemBioChem* **14**, 1943-1948

48. Götz, A., and Scharnagl, C. (2018) Dissecting conformational changes in APP's transmembrane domain linked to ϵ-efficiency in familial Alzheimer's Disease. *PLoS One* **13**, e0200077

49. Tolia, A., Chavez-Gutierrez, L., and De Strooper, B. (2006) Contribution of presenilin transmembrane domains 6 and 7 to a water-containing cavity in the γ-secretase complex. *J Biol Chem* **281**, 27633-27642

50. Buck, M. (1998) Trifluoroethanol and colleagues: cosolvents come of age. Recent studies with peptides and proteins. *Q Rev Biophys* **31**, 297-355

51. Schutz, C. N., and Warshel, A. (2001) What are the dielectric "constants" of proteins and how to validate electrostatic models? in *Proteins: Structure, Function and Genetics*

52. Edbauer, D., Winkler, E., Regula, J. T., et al. (2003) Reconstitution of γ-secretase activity. *Nat Cell Biol* **5**, 486-488

53. Kretner, B., Trambauer, J., Fukumori, A., et al. (2016) Generation and deposition of Aβ43 by the virtually inactive presenilin-1 L435F mutant contradicts the presenilin loss-of-function hypothesis of Alzheimer's disease. *EMBO Mol Med* **8**, 458-465

54. Shearman, M. S., Beher, D., Clarke, E. E., et al. (2000) L-685,458, an aspartyl protease transition state mimic, is a potent inhibitor of amyloid b-protein precursor γ-secretase activity. *Biochemistry* **39**, 8698-8704.

55. Barrett, P. J., Song, Y., Van Horn, W. D., et al. (2012) The amyloid precursor protein has a flexible transmembrane domain and binds cholesterol. *Science* **336**, 1168-1171

56. Poschner, B. C., Quint, S., Hofmann, M. W., et al. (2009) Sequence-specific conformational dynamics of model transmembrane domains determines their membrane fusogenic function. *J Mol Biol* **386**, 733-741

57. Stelzer, W., Poschner, B. C., Stalz, H., et al. (2008) Sequence-specific conformational flexibility of SNARE transmembrane helices probed by hydrogen/deuterium exchange. *Biophys J* **95**, 1326-1335

58. Konermann, L., Pan, J., and Liu, Y.-H. (2011) Hydrogen exchange mass spectrometry for studying protein structure and dynamics. *Chem Soc Rev* **40**, 1224-1234

59. Audagnotto, M., Kengo Lorkowski, A., and Dal Peraro, M. (2018) Recruitment of the amyloid precursor protein by γ-secretase at the synaptic plasma membrane. *Biochem Biophys Res Commun* **498**, 334-341

60. Götz, A., Högel, P., Silber, M., et al. (2018) Increased γ-sites H-bond stability relates to altered ε-efficiency and Aβ levels in the I45T familial Alzheimer's Disease mutant of APP. *BioRxiv* **372698**, doi.org/10.1101/372698

61. Teilum, K., Kragelund, B. B., and Poulsen, F. M. (2005) Application of hydrogen exchange kinetics to studies of protein folding. Weinheim: Wiley-VCH. pp 634-672

62. Killian, J. A. (1998) Hydrophobic mismatch between proteins and lipids in membranes. *Biochim Biophys Acta* **1376**, 401-415

63. Strandberg, E., Esteban-Martín, S., Salgado, J., et al. (2009) Orientation and dynamics of peptides in membranes calculated from 2H-NMR data. *Biophys J* **96**, 3223-3232

64. Strandberg, E., Esteban-Martin, S., Ulrich, A. S., et al. (2012) Hydrophobic mismatch of mobile transmembrane helices: Merging theory and experiments. *Biochim Biophys Acta* **1818**, 1242-1249

65. Esteban-Martin, S., and Salgado, J. (2007) The dynamic orientation of membrane-bound peptides: bridging simulations and experiments. *Biophys J* **93**, 4278-4288

66. van der Wel, P. C., Strandberg, E., Killian, J. A., et al. (2002) Geometry and intrinsic tilt of a tryptophan-anchored transmembrane α-helix determined by (2)H NMR. *Biophys J* **83**, 1479-1488

67. Itkin, A., Salnikov, E. S., Aisenbrey, C., et al. (2017) Structural characterization of the amyloid precursor protein transmembrane domain and its γ-cleavage site. *ACS Omega* **2**, 6525-6534

68. Bugge, K., Lindorff-Larsen, K., and Kragelund, B. B. (2016) Understanding single-pass transmembrane receptor signaling from a structural viewpoint-what are we missing? *FEBS J* **283**, 4424-4451

69. Wilman, H. R., Shi, J., and Deane, C. M. (2014) Helix kinks are equally prevalent in soluble and membrane proteins. *Proteins* **82**, 1960-1970

70. Hall, S. E., Roberts, K., and Vaidehi, N. (2009) Position of helical kinks in membrane protein crystal structures and the accuracy of computational prediction. *J Mol Graph Modelling* **27**, 944-950

71. Hayward, S. (1999) Structural principles governing domain motions in proteins. *Proteins* **36**, 425-435

72. Hayward, S., and Lee, R. A. (2002) Improvements in the analysis of domain motions in proteins from conformational change: DynDom version 1.50. *J Mol Graph Model* **21**, 181-183

73. Wassenaar, T. A., Pluhackova, K., Moussatova, A., et al. (2015) High-throughput simulations of dimer and trimer assembly of membrane proteins. The DAFT approach. *J Chem Theory Comput* **11**, 2278-2291

74. Altwaijry, N. A., Baron, M., Wright, D. W., et al. (2017) An ensemble-based protocol for the computational prediction of helix-helix interactions in G protein-

coupled receptors using coarse-grained molecular dynamics. *J Chem Theory Comput* **13**, 2254-2270

75. Poma, A. B., Cieplak, M., and Theodorakis, P. E. (2017) Combining the MARTINI and structure-based coarse-grained approaches for the molecular dynamics studies of conformational transitions in proteins. *J Chem Theory Comput* **13**, 1366-1374

76. Li, S., Zhang, W., and Han, W. (2017) Initial substrate binding of γ-secretase: The role of substrate flexibility. *ACS Chem Neurosci* **8**, 1279-1290

77. Brown, M. C., Abdine, A., Chavez, J., et al. (2018) Unwinding of the Substrate Transmembrane Helix in Intramembrane Proteolysis. *Biophys J* **114**, 1579-1589

78. Nadezhdin, K. D., Bocharova, O. V., Bocharov, E. V., et al. (2011) Structural and dynamic study of the transmembrane domain of the amyloid precursor protein. *Acta Naturae* **3**, 69-76

79. Miyashita, N., Straub, J. E., Thirumalai, D., et al. (2009) Transmembrane structures of amyloid precursor protein dimer predicted by replica-exchange molecular dynamics simulations. *J Am Chem Soc* **131**, 3438-3439

80. Dominguez, L., Foster, L., Straub, J. E., et al. (2016) Impact of membrane lipid composition on the structure and stability of the transmembrane domain of amyloid precursor protein. *Proc Natl Acad Sci U S A* **113**, E5281-5287

81. Cao, Z., Hutchison, J. M., Sanders, C. R., et al. (2017) Backbone hydrogen bond strengths can vary widely in transmembrane helices. *J Am Chem Soc* **139**, 10742-10749

82. Henzler-Wildman, K. A., Lei, M., Thai, V., et al. (2007) A hierarchy of timescales in protein dynamics is linked to enzyme catalysis. *Nature* **450**, 913-916

83. Nashine, V. C., Hammes-Schiffer, S., and Benkovic, S. J. (2010) Coupled motions in enzyme catalysis. *Curr Opin Chem Biol* **14**, 644-651

84. Ma, B., and Nussinov, R. (2010) Enzyme dynamics point to stepwise conformational selection in catalysis. *Curr Opin Chem Biol* **14**, 652-659

85. Boehr, D. D., Nussinov, R., and Wright, P. E. (2009) The role of dynamic conformational ensembles in biomolecular recognition. *Nat Chem Biol* **5**, 789-796

86. Warshel, A., and Bora, R. P. (2016) Perspective: Defining and quantifying the role of dynamics in enzyme catalysis. *J Chem Phys* **144**, 180901

87. Agarwal, P. K., Doucet, N., Chennubhotla, C., et al. (2016) Conformational Sub-states and Populations in Enzyme Catalysis. *Meth Enzymol* **578**, 273-297

88. Guo, Z. Y., Kraka, E., and Cremer, D. (2013) Description of local and global shape properties of protein helices. *J Mol Model* **19**, 2901-2911

89. Deatherage, C. L., Lu, Z., Kroncke, B. M., et al. (2017) Structural and biochemical differences between the Notch and the amyloid precursor protein transmembrane domains. *Sci Adv* **3**, e1602794

90. Li, Q., Wong, Y. L., and Kang, C. (2014) Solution structure of the transmembrane domain of the insulin receptor in detergent micelles. *Biochim Biophys Acta* **1838**, 1313-1321

91. Lezon, T. R., and Bahar, I. (2010) Using entropy maximization to understand the determinants of structural dynamics beyond native contact topology. *PLoS Comput Biol* **6**, e1000816

92. Palmer, A. G., 3rd. (2015) Enzyme dynamics from NMR spectroscopy. *Acc Chem Res* **48**, 457-465

93. Anthis, N. J., and Clore, G. M. (2015) Visualizing transient dark states by NMR spectroscopy. *Q Rev Biophys* **48**, 35-116

94. Shirotani, K., Tomioka, M., Kremmer, E., et al. (2007) Pathological activity of familial Alzheimer's disease-associated mutant presenilin can be executed by six different γ-secretase complexes. *Neurobiol Dis* **27**, 102-107

95. Page, R. C., Kim, S., and Cross, T. A. (2008) Transmembrane helix uniformity examined by spectral mapping of torsion angles. *Structure* **16**, 787-797

96. Winkler, E., Hobson, S., Fukumori, A., et al. (2009) Purification, pharmacological modulation, and biochemical characterization of interactors of endogenous human γ-secretase. *Biochemistry* **48**, 1183-1197

97. Koos, M. R. M., Kummerlowe, G., Kaltschnee, L., et al. (2016) CLIP-COSY: A clean In-phase experiment for the rapid acquisition of COSY-type correlations. *Angew Chem Int Edit* **55**, 7655-7659

98. Munowitz, M. G., Griffin, R. G., Bodenhausen, G., et al. (1981) Two-dimensional rotational spin-echo nuclear magnetic resonance in solids: correlation of chemical shift and dipolar interactions. *J Am Chem Soc* **103**, 2529-2533

99. Huster, D., Xiao, L., and Hong, M. (2001) Solid-state NMR investigation of the dynamics of the soluble and membrane-bound colicin Ia channel-forming domain. *Biochemistry* **40**, 7662-7674

100. Sparks, K. A., Gleason, N. J., Gist, R., et al. (2014) Comparisons of interfacial Phe, Tyr, and Trp residues as determinants of orientation and dynamics for GWALP transmembrane peptides. *Biochemistry* **53**, 3637-3645

101. Thibado, J. K., Martfeld, A. N., Greathouse, D. V., et al. (2016) Influence of high pH and cholesterol on single arginine-containing transmembrane peptide helices. *Biochemistry* **55**, 6337-6343

102. Rankenberg, J. M., Vostrikov, V. V., DuVall, C. D., et al. (2012) Proline kink angle distributions for GWALP23 in lipid bilayers of different thicknesses. *Biochemistry* **51**, 3554-3564

103. Vostrikov, V. V., Daily, A. E., Greathouse, D. V., et al. (2010) Charged or aromatic anchor residue dependence of transmembrane peptide tilt. *J Biol Chem* **285**, 31723-31730

104. Vogel, A., Reuther, G., Roark, M. B., et al. (2010) Backbone conformational flexibility of the lipid modified membrane anchor of the human N-Ras protein investigated by solid-state NMR and molecular dynamics simulation. *Biochim Biophys Acta* **1798**, 275-285

105. Xiao, H., Hoerner, J. K., Eyles, S. J., et al. (2005) Mapping protein energy landscapes with amide hydrogen exchange and mass spectrometry : I . A generalized model for a two-state protein and comparison with experiment. *Protein Science* **14**, 543-557

106. Phillips, J. C., Braun, R., Wang, W., et al. (2005) Scalable molecular dynamics with NAMD. *J Comput Chem* **26**, 1781-1802

107. Best, R. B., Zhu, X., Shim, J., et al. (2012) Optimization of the additive CHARMM all-atom protein force field targeting improved sampling of the backbone ϕ, ψ and side-chain χ_1 and χ_2 dihedral angles. *J Chem Theory Comput* **8**, 3257-3273

108. Lee, J., Cheng, X., Swails, J. M., et al. (2016) CHARMM-GUI input generator for NAMD, GROMACS, AMBER, OpenMM, and CHARMM/OpenMM simulations using the CHARMM36 additive force field. *J Chem Theory Comput* **12**, 405-413

109. Humphrey, W., Dalke, A., and Schulten, K. (1996) VMD: Visual molecular dynamics. *Journal of Molecular Graphics & Modelling* **14**, 33-38

110. Diciccio, T., and Tibshirani, R. (1987) Better bootstrap confidence-intervals - comment. *J Am Stat Assoc* **82**, 187-188

111. Monticelli, L., Kandasamy, S. K., Periole, X., et al. (2008) The MARTINI coarse-grained force field: Extension to proteins. *Journal of Chemical Theory and Computation* **4**, 819-834

112. Wolek, K., Gomez-Sicilia, A., and Cieplak, M. (2015) Determination of contact maps in proteins: A combination of structural and chemical approaches. *J Chem Phys* **143**, 243105

113. Berendsen, H. J. C., Vanderspoel, D., and Vandrunen, R. (1995) Gromacs - a message-passing parallel molecular-dynamics implementation. *Comput Phys Commun* **91**, 43-56

114. de Jong, D. H., Singh, G., Bennett, W. F. D., et al. (2013) Improved parameters for the martini coarse-grained protein force field. *J Chem Theory Comput* **9**, 687-697